Molecular Therapy
Nucleic Acids
Original Article

Restoration of myogenesis in ALS-myocytes through miR-26a-5p-mediated Smad4 inhibition and its impact on motor neuron development

Caterina Peggion,[1] Raphael Severino Bonadio,[1] Roberto Stella,[2] Silvia Scalabrin,[1] Laura Pasetto,[3] Caterina Millino,[1] Laura Camporeale,[3] Beniamina Pacchioni,[1] Valentina Bonetto,[3] Alessandro Bertoli,[4,5,6] Stefano Cagnin,[1,7] and Maria Lina Massimino[6]

[1]Department of Biology, University of Padova, 35131 Padova, Italy; [2]Department of Chemistry, Istituto Zooprofilattico Sperimentale delle Venezie, 35020 Legnaro, Padova, Italy; [3]Research Center for ALS, Istituto di Ricerche Farmacologiche Mario Negri IRCCS, 20156 Milan, Italy; [4]Department of Biomedical Sciences, University of Padova, 35131 Padova, Italy; [5]Padova Neuroscience Center, University of Padova, 35131 Padova, Italy; [6]Neuroscience Institute, Section of Padova, National Research Council (CNR), 35131 Padova, Italy; [7]CIR-Myo Myology Center, University of Padova, 35131 Padova, Italy

Amyotrophic lateral sclerosis (ALS) is the most common adult-onset paralytic disorder, characterized primarily by a progressive loss of motor neurons (MNs) in which degeneration skeletal muscle involvement has been demonstrated. Skeletal muscle is a plastic tissue that responds to insults through proliferation and differentiation of satellite cells. Skeletal muscle degeneration and regeneration are finely regulated by signals that regulate satellite cell proliferation and differentiation. It is known that satellite cell differentiation is impaired in ALS, but little is known about the involvement of microRNAs (miRNAs) and their role in intercellular communication in ALS. Here we demonstrated impaired differentiation of satellite cells derived from ALS mice related to the impairment of myogenic p38MAPK and protein kinase A (PKA)/pCREB signaling pathways that can be regulated by miR-882 and -134-5p. These miRNAs participate in autocrine signaling in association with miR-26a-5p that, secreted from wild-type (WT) and captured by ALS myoblasts, enhances ALS-related myoblast differentiation by repressing Smad4-related signals. Moreover, miR-26a-5p and -431-5p work in a paracrine way ameliorating motoneuron differentiation. These findings emphasize the need to better understand intercellular communication and its role in ALS pathogenesis and progression. They also suggest that miRNAs could be targeted or used as therapeutic agents for myofiber and MN regeneration.

INTRODUCTION

Amyotrophic lateral sclerosis (ALS) is a devastating motoneuronal disorder characterized by the progressive loss of motor neurons (MNs) with a worldwide incidence of 0.6–3.8/100,000 persons-per-year and a prevalence that ranges from 4.1 to 8.4 per 100,000 people.[1] The hallmark of ALS is the selective and progressive degeneration of the lower and upper MNs, resulting in spasticity, hyperexcitability, muscle atrophy, and weakness. Eventually, this leads to paralysis that, in 50% of affected individuals, causes death within 2–5 years of symptom onset.[2]

Most cases of ALS (about 90%–95%) have no known cause and are defined as sporadic ALS. However, genetics and various environmental factors are recognized as risk factors for the disease. Less than 5%–10% of ALS cases have a genetic cause (familial ALS; fALS), mainly with an autosomal dominant pattern of inheritance.[3,4] The first gene whose mutations were associated to fALS was the Cu/Zn superoxide dismutase 1 (SOD1), identified 30 years ago.[5] Since then, more than 40 genes have been associated with ALS (both fALS and sALS),[6] including the most common C9orf72, TARDBP (encoding the protein TDP-43) and FUS/TLS (coding for the protein FUS).[7]

The identification of fALS-related mutations has paved the way for numerous studies to unveil the pathomechanisms of ALS, mainly through cellular or transgenic (Tg) rodent models, among which the earliest and historically most exploited is Tg mice overexpressing the SOD1 missense mutation (G93A) linked to human ALS.[8] Studies based on a such models permitted to propose perturbations in (1) protein quality control and homeostasis[9]; (2) RNA homeostasis and trafficking[10]; (3) cytoskeletal dynamics[11]; and (4) mitophagy and mitochondrial dysfunctions[12,13] as important mechanism for ALS development or progression. The majority of such studies were driven by a "neuro-centric" perspective, which posited that MN dysfunctions were the primary cause of the disease. Conversely,

Received 15 August 2024; accepted 28 May 2025;
https://doi.org/10.1016/j.omtn.2025.102581.

Correspondence: Stefano Cagnin. Department of Biology, University of Padova, 35131 Padova, Italy.
E-mail: stefano.cagnin@unipd.it
Correspondence: Maria Lina Massimino. Neuroscience Institute, Section of Padova, National Research Council (CNR), Padova 35131, Italy.
E-mail: marialina.massimino@cnr.it

alterations in skeletal muscle or other cell types were viewed as mere consequences of MN loss. Growing evidences, however, suggest that non-cell-autonomous events elicited by non-neuronal cells, such as astrocytes, microglia, and peripheral blood mononuclear cells, contribute to MN degeneration and ALS onset and progression.[12,14–17] Different data support the active participation of skeletal muscle in MN death in ALS and have given rise to an opposite and still debated "muscle-centric" perspective, according to which pathological changes in skeletal muscle cells or muscular toxicity drive or contribute to denervation and MN loss.[14,15,18–20]

Differently from neurons in central nervous system, myofibers of skeletal muscle that degenerate during ALS progression[21] are capable of regenerating thanks to a population of adult stem cells called satellites cells. Several data support satellite cell involvement in ALS development both in animal models[22–25] and patients.[26] Moreover, satellite cells are activated in ALS patients' biopsies before the onset of clear neurological symptoms[24,25] supporting the idea that satellite cell dysfunction may contribute to ALS pathology, perhaps exacerbating neuromuscular junction (NMJ) dysfunction.[27] Myogenic program of satellite cells is tightly regulated by a broad spectrum of signaling molecules (i.e., hormones, cytokines, and peptides) that act in a paracrine/autocrine manner by regulating a series of transcription factors (TFs) or chromatin-remodelling factors.[28] In addition, circulating and exosome-derived microRNAs (miRNAs) have been found to be important players in the regulation of skeletal muscle development and differentiation.[29]

In the present study, we demonstrate that primary cultures of myocytes (PCM), derived from pre-phenotypic condition of ALS-related human SOD1 G93A mutant (hSOD1(G93A)) transgenic mice, are characterized by an impaired/delayed myogenesis due to the altered activation of the p38 MAP kinase signaling axis and of myogenic regulatory factors (MRF). Considering the importance of cell communication in muscle development and repair and the involvement of miRNAs in ALS, we used a transcriptomic approach to demonstrate that PCM from human SOD1 wild-type (hSOD1(WT)) secrete different miRNAs from hSOD1(G93A) PCM. Interestingly, we showed that miRNAs secreted by hSOD1 (G93A) PCM (miR-134-5p and miR-882) hinder differentiation by targeting important regulators of positive myoblast differentiation such as Pax7, Creb1, and p38. Conversely, miR-26a, secreted by hSOD1(WT) PCM, targets Igfbp5 and Smad4 stimulating differentiation. Therefore, miR-26a, secreted from healthy myoblasts, improves myogenesis of hSOD1(G93A) cells through inhibition of Smad4 and its regulated genes. Notably, the same miRNA, and miR-431-5p, facilitates the differentiation of MNs, enabling elongation of neurites and their branching.

This experimental evidence supports that deregulation of circulating miRNAs plays a role in myocyte (re)programming and MN development in ALS and opens new avenues for the identification of RNA-based therapeutic molecules designed to stimulate muscle regeneration in patients with ALS.

RESULTS

Primary myocytes derived from hSOD1(G93A) mice show altered expression of myogenic regulatory factors and impaired activation of p38 MAPK signaling program

We already demonstrated that during *in vitro* differentiation PCM derived from ALS-related hSOD1(G93A) mice showed impaired differentiation compared to the hSOD1(WT) counterpart.[30] To molecularly investigate this phenotype, we evaluated biochemical parameters during PCM differentiation. The expression of EmbMyHC began to be appreciable at 3 days *in vitro* (DIV) in both hSOD1(G93A) and hSOD1(WT) PCM cells, but hSOD1 (G93A) myotubes expressed remarkably less EmbMyHC than hSOD1(WT) from 3 to 6 DIV (Figure 1A). We also evaluated the expression of Pax7, MyoD, and myogenin (Figure 1A), crucial TFs that, in concert with others, orchestrate myocyte proliferation and differentiation.[31] Despite all three TFs had the expected expression trend during *in vitro* myogenesis, they behaved differently in PCM with different hSOD1 genotypes. Pax7 and MyoD showed significant reduction at 2 DIV in hSOD1(G93A) PCM compared with controls, while myogenin reduction was detected at 3 DIV (Figure 1A). In summary, the proteins that should increase in abundance during differentiation in hSOD1(G93A) PCM do not increase sufficiently, while the one that should decrease (Pax7) decreases faster than normal.

We also monitored the expression and/or activation state of other TFs and kinases critical for myoblast proliferation and differentiation. p38 mitogen-activated protein kinase (MAPK), which is fundamental for early stages of myogenesis[32,33] was less phosphorylated in hSOD1(G93A) cells (Figure 1B), while Akt, known to promote later muscle differentiation stages,[34] did not show significant differences in the two genotypes (Figure S1). The expression of cyclin dependent kinase inhibitor 1A (p21), which is regulated by and acts downstream of MyoD to maintain a postmitotic state, was reduced in hSOD1 (G93A) PCM (Figure 1B). In addition, hSOD1(G93A) PCM exhibits reduced phosphorylation of the protein kinase A (PKA) substrates (Figure 1C). In support of this evidence, we showed that cAMP-responsive element-binding protein (CREB), that is phosphorylated by PKA, was less phosphorylated in hSOD1(G93A) PCM. CREB is essential for transcription of various myogenic TFs, including MyoD itself[35] (Figure 1D).

Factors secreted by hSOD1(WT) myocytes rescued the myogenic differentiation of hSOD1(G93A) cells

To investigate intercellular communication in myogenic cells of skeletal muscle and its impacts on hSOD1(G93A) PCM differentiation, we utilized a co-culture system that eliminates physical contact of cells with a different genotype (Figure S2). Myotubes derived from the hSOD1(G93A) myoblasts in co-culture with hSOD1(WT) ($G93A_{WT}$) were more similar to controls (WT_{WT}) and formed much longer and bulkier myotubes than when co-cultured with isogenic hSOD1(G93A) myoblasts ($G93A_{G93A}$) (Figure 2A). This observation was confirmed by quantitative analyses of myotube

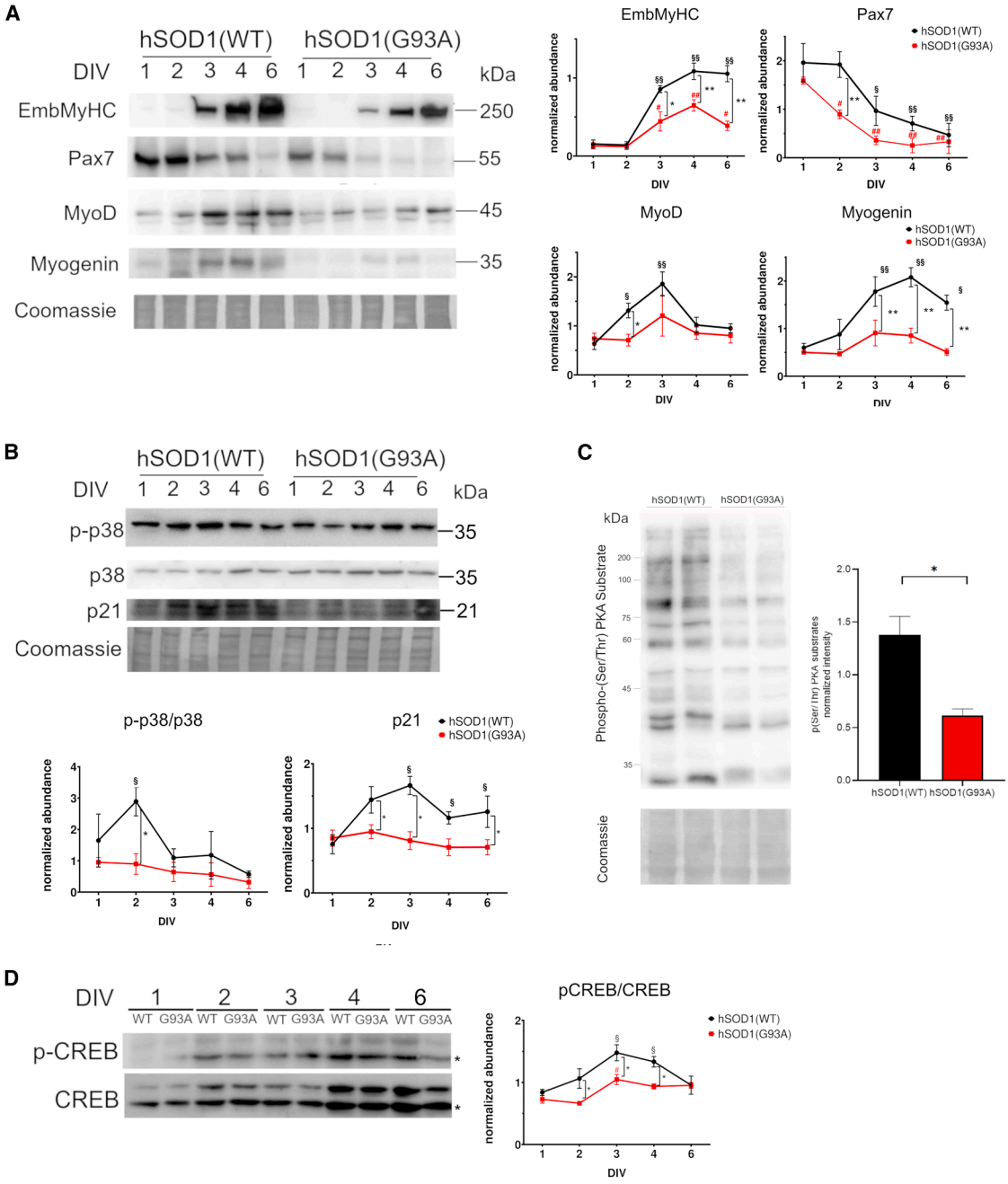

Figure 1. PCM derived from muscles of hSOD1(G93A) Tg mice show impaired *in vitro* differentiation compared to the hSOD1(WT) counterpart

(A) The expression of EmbMyHC, Pax7, MyoD, and myogenin was evaluated by WB in hSOD1(WT) and hSOD1(G93A) PCM at different DIV. The left shows representative WBs and the corresponding Coomassie blue staining of the membrane, while the graphs on the right report the densitometric analysis for each protein. $n = 3$ for each DIV and hSOD1 genotype. (B) p38 (MAPK) phosphorylation (Thr180/Tyr182) and the expression of p21 were analyzed by WB at different DIV. The top shows representative WBs, and the graphs on the bottom show the corresponding densitometric analysis by reporting the ratio between phosphorylated and total protein amounts for p38 while the abundance of p21 was determined by normalizing the optical density of immunoreactive bands to that of the corresponding Coomassie blue-stained lanes. $n = 4$ (different PCM) for each DIV and hSOD1 genotype. (C) 4 DIV PCM protein extracts were analyzed for phosphorylation of PKA substrates by WB using α-pPKAs as antibody. Loading control with the Coomassie blue staining. $n = 4$ (different PCM) for each DIV and hSOD1 genotype. (D) CREB phosphorylation (Ser133) was analyzed by WB at different DIV.

(legend continued on next page)

area (Figures 2B and 2C), differentiation index, (Figure 2D), fusion index (Figure 2E), and the expression of EmbMyHC (Figure 2F).

Furthermore, we demonstrated that altered expression of myogenin (Figure 1A) and abnormal CREB activation in hSOD1(G93A) myocytes (Figure 1D) were restored by co-culture of hSOD1(G93A) PCM with WT counterpart (Figure 2G). All such parameters further support the idea that secreted molecules by hSOD1(WT) myocytes aided hSOD1(G93A) cells to recover a correct myogenic program.

To understand if secreted factors influence myogenic differentiation during early or late stages of *in vitro* culturing, we analyzed the expression of EmbMyHC, the differentiation and fusion index in 4 DIV hSOD1(G93A) cells in which the transwell inserts were kept only for 2 DIV or maintained for the total culturing period (4 DIV). The abundance of EmbMyHC (Figure S3A), the differentiation index (Figure S3B), and the fusion index (Figure S3C) were comparable between the two considered conditions. This indicates that factors implicated in the communication between cells influencing myodifferentiation are early secreted.

Since miRNAs have been found to regulate myogenesis, our results prompted us to unveil whether an alteration in secreted miRNAs could explain crosstalk between PCMs bearing two different hSOD1 genotypes and the differential myogenesis.

hSOD1(G93A) myocytes secrete different miRNAs from their WT counterpart

We characterized secreted miRNA signature in hSOD1(WT) and hSOD1(G93A) myotubes. A total of 492 miRNAs were identified in the culture medium, and 53 miRNAs showed differential expression under the conditions considered. Hierarchical clustering reveals that WT_{WT} and $G93A_{WT}$ conditions cluster together, whereas the $G93A_{G93A}$ co-cultures form a separate sample cluster (Figure 3A). This strongly suggests different behavior of hSOD1(G93A) PCM respect to the WT and that the phenotypic rescue of atrophic myotubes may be mediated by miRNAs secreted by the hSOD1(WT) cells. Differentially expressed miRNAs were divided into two big clusters: the first comprising miRNAs more expressed in the medium of the WT_{WT} co-culture and less expressed in the $G93A_{G93A}$ co-culture (blue cluster in Figure 3A), while the second encompasses the opposite condition (violet cluster in Figure 3A). To confirm miRNA transcriptomic analysis, we validated the expression of six miRNAs by RT-qPCR: miR-26a-5p, -324-5p, and -431-5p within the blue cluster and miR-28a-3p, -882, and -134-5p within the violet cluster. We confirmed the reduced expression of miR-26a-5p, -324-5p, and -431-5p in the medium derived from $G93A_{G93A}$ co-culture in comparison with WT_{WT} co-culture (Figure 3B). We also confirmed the increased expression of miR-28a-3p, -882, and -134-5p in the $G93A_{G93A}$ condition (Figure 3C).

miR-134-5p, -882, and -26a-5p affect the expression of genes related to myogenesis

To fully understand miRNA activity, we need to explore their interactions with target molecules. In the cluster representing miRNAs enriched in the $G93A_{G93A}$ medium, only miR-28a-3p, -882, -711, -200a-5p, and -134-5p have target genes involved in the striated muscle functions (indicated with @ in Figure 3A). Differently, in the cluster representing miRNAs enriched in the WT_{WT} medium, 10 miRNAs have target genes involved in the striated muscle functions (indicated with # in Figure 3A).

Among the interactions between miRNAs and their targets described in Figure S4 and Table S3, luciferase assays were eployed to validate the interactions between miR-134-5p and *Creb1* (Figure 4A), miR-26a-5p and *Igfbp5* (Figure 4B), miR-882 and *Pax7*, and miR-882 and *MyoD1* (Figure 4C). The interactions between miR-134-5p and *Creb1* and miR-26a-5p and *Igfbp5* were validated because indicated as weak in considered databases (Table S3) and because the significance of targets in muscle and axon growth and maintenance.[36,37] The interactions between miR-882 and *Pax7* and *MyoD1* were validated due to the importance of the targets in myoblast differentiation.

Moreover, to better understand the function of secreted miRNAs that can mediate intercellular communication, we transfected C2C12 cells using synthetic miR-26a-5p, -134-5p, and -882 molecules obtaining their consistent upregulation (Figure 4D). miRNA upregulation induced the downregulation of each miRNA target after 24 h of transfection and additional 24 h of cell recovery (Figures 4E–4G).

Secreted miRNAs regulate genes in target cells

Can secreted miRNAs be internalized by cells to regulate the expression of target genes through a paracrine mechanism? We analyzed whether the concentration of secreted miRNAs changes in target cells (Figure S2 for an explanation of experimental design). We showed that miR-26a-5p is the most highly expressed miRNA in hSOD1(WT) PCM cells followed by miR-431-5p (Figure 5A). Differently, miR-28a-3p is the miRNA most expressed in hSOD1(G93A) PCM cells. Considering the communication between PCM cells, miR-431-5p, -26a-5p, and -324-5p expression increases within hSOD1(G93A) PCM co-cultured with hSOD1(WT) cells in comparison with the co-culture with hSOD1(G93A) PCM (Figure 5A). This confirms that WT cells are responsible for the secretion of such miRNAs and that they can be captured by "accepting" co-cultured cells. This was also confirmed by the overexpression of these miRNAs in hSOD1(WT) cells when co-cultured with hSOD1(WT) PCM

The left shows representative WBs, and the graph on the right show the corresponding densitometric analysis by reporting the ratio between phosphorylated and total protein amount. $n = 4$ (different PCM) for each DIV and hSOD1 genotype. * indicates bands considered for protein quantification. In (A, B, and D), $^{*}p < 0.05$ and $^{**}p < 0.01$, hSOD1 (WT) vs. hSOD1(G93A) in each DIV; §$p < 0.05$ and §§$p < 0.01$ with respect to hSOD1(WT) in 1 DIV; and #$p < 0.05$ and ##$p < 0.01$ with respect to hSOD1(G93A) in 1 DIV; two-way ANOVA followed by Sidak's multiple comparison test. In (C), $^{*}p < 0.05$, Mann-Whitney test.

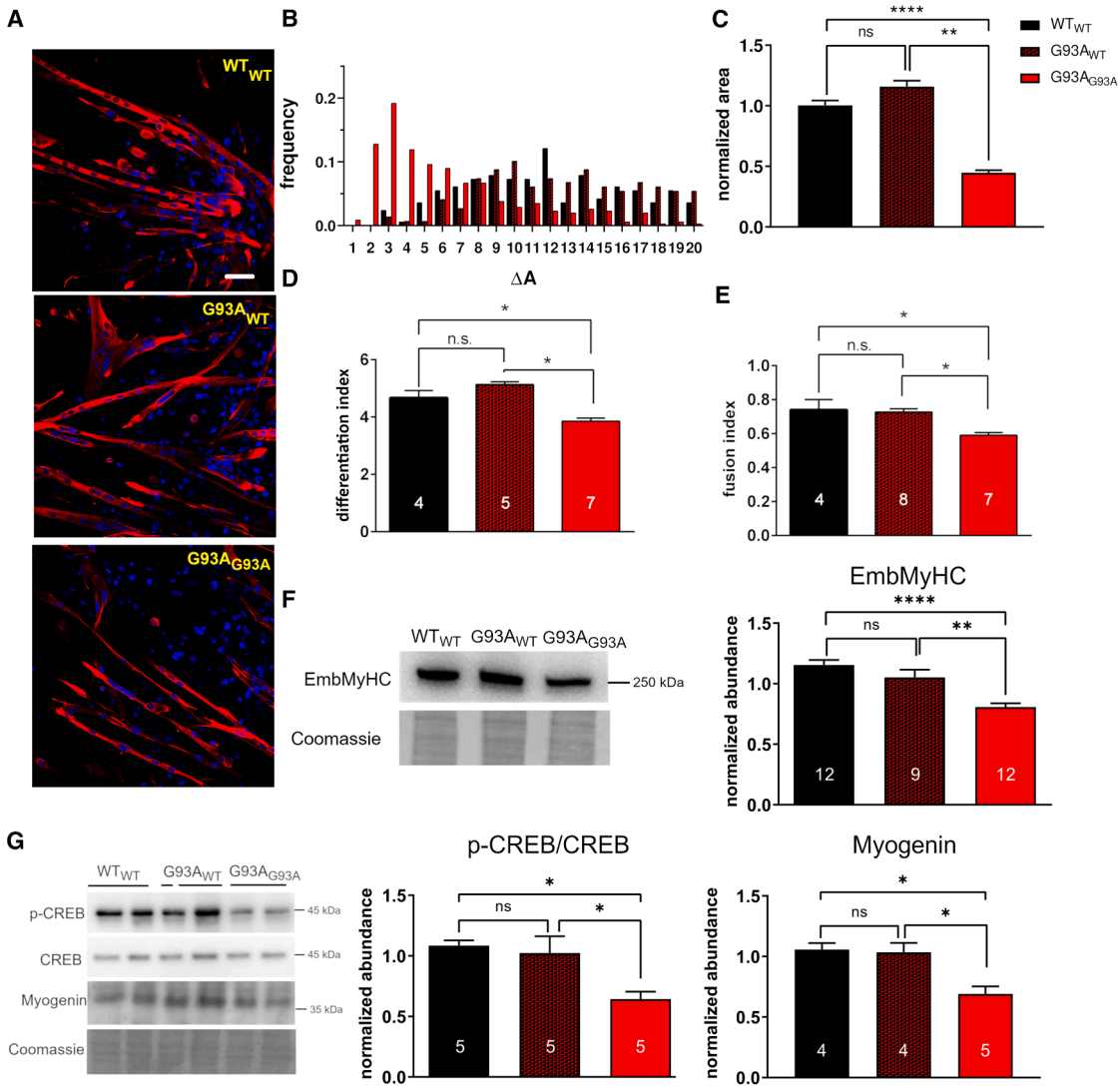

Figure 2. hSOD1(G93A) co-cultured with hSOD1(WT) PCM recover the defective differentiation phenotype

(A) Representative fluorescent images of the three different co-culture conditions (WT_{WT}, top; WT_{G93A}, middle; and $G93A_{G93A}$, bottom) (see Figure S2). At 4 DIV, target cells were co-stained with anti-desmin antibody (red signal) and the Hoechst 33342 dye (blue signal). Scale bars, 20 μm. (B) The graph reports the frequency distribution of the myotube area under the three different culturing conditions. (C) The diagram reports the average myotube area in the three co-culture settings normalized to the mean value of the WT_{WT} cultures. $n = 21$ for WT_{WT} and WT_{G93A}, while is 35 for $G93A_{G93A}$. (D and E) The bar diagrams show the differentiation index and the fusion index under the three co-culture conditions. (F) At 4 DIV, the EmbMyHC expression was assessed by WB in the three co-culture conditions. The left shows a representative WB and the corresponding Coomassie blue staining of the membrane, while graphs on the right report the densitometric analysis. (G) The activation of CREB and the expression of myogenin were assessed at 4 DIV co-cultures by WB as described in Figure 1. The left shows representative WBs and the corresponding Coomassie staining of the membrane, while the bar diagrams on the right show the corresponding densitometric analysis. n is reported inside the bars. For all panels, n.s., not significant, $^{*}p < 0.05$ $^{**}p < 0.01$, and $^{****}p < 0.0001$. One-way ANOVA followed by Tukey's multiple comparison test.

(Figure 5A). Conversely, we showed that miR-28a-3p, -882, and -134-5p are secreted from hSOD1(G93A) myocytes. In fact, their expression increases in tested cells when they are co-cultured with cells with hSOD1(G93A) genotype (Figure 5A).

Because we confirmed the interactions between miRNAs and their targets by luciferase assay and the ability of secreted miRNAs to enter target cells, we decided to test the expression of miRNA targets in PCM derived from hSOD1(G93A) mice co-cultured with hSOD1 (G93A) or hSOD1(WT) PCM and in PCM derived from hSOD1 (WT) mice co-cultured as previously described for hSOD1(G93A) PCM. Igfbp5 was downregulated in hSOD1(G93A) PCM when co-cultured with WT cells supporting our previous findings about the activity of miR-26a-5p (Figure 5B). Similarly, the expressions of

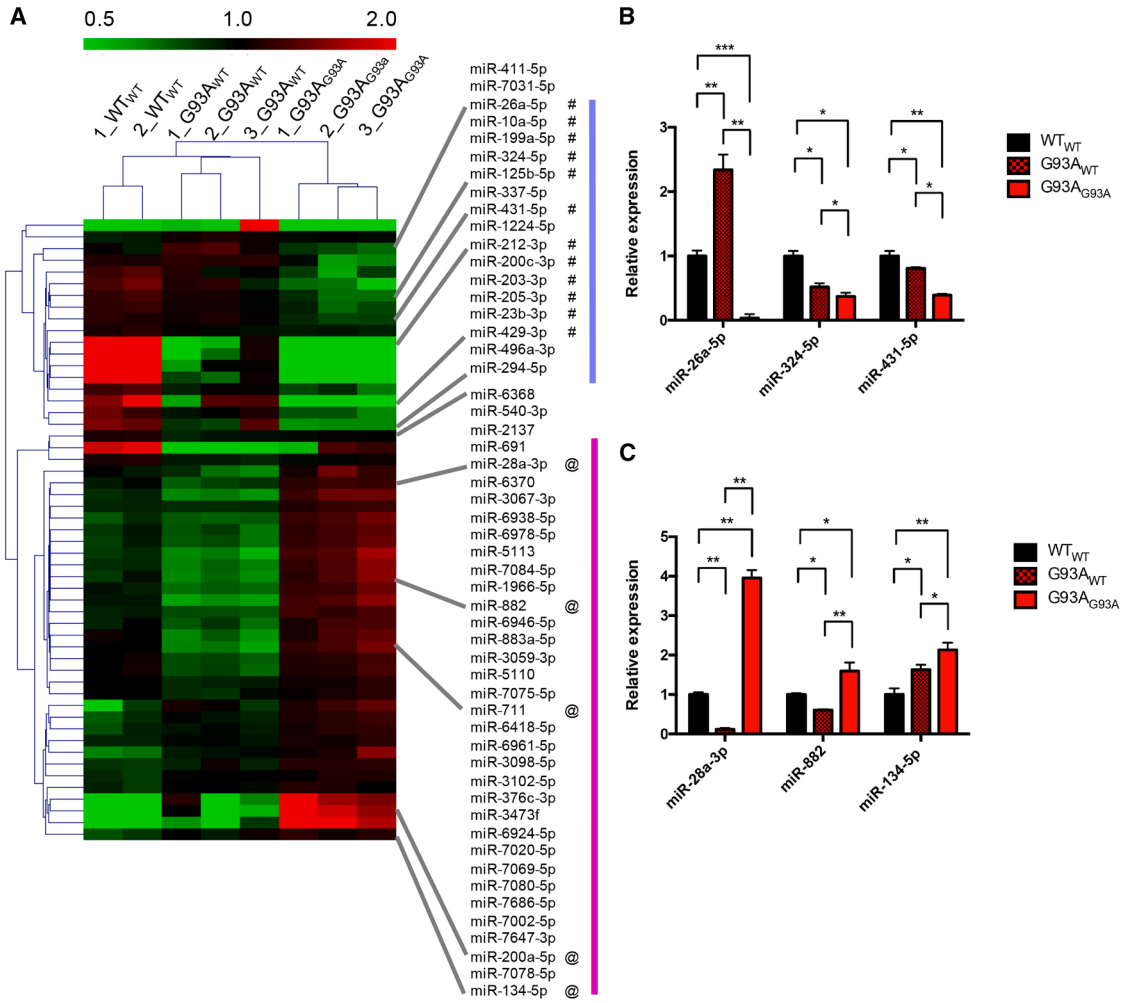

Figure 3. miRNA expression

(A) Heatmap of differentially expressed miRNAs in the medium derived from the conditions described in the sample names (columns). The expression of each miRNA is indicated as relative to the average of the miRNA in the samples. Biological replicates cluster together and $G93A_{G93A}$ samples cluster separated from WT_{WT} and $G93A_{WT}$. On the right, it is shown miRNA cluster with a low expression in the $G93A_{G93A}$ sample (blue) and the one with high expression in $G93A_{G93A}$ (violet). # and @ indicate miRNAs associated with striated muscle functions according to target function. (B) Relative expression of miRNAs within the blue cluster according to RT-qPCR experiments. (C) Relative expression of miRNAs within the violet cluster according to RT-qPCR. For both (B and C) $^{*}p < 0.05$, $^{**}p < 0.005$, and $^{***}p < 0.0005$ calculated according to t test between indicated samples considering unequal variance. SD is indicated.

Pax7 and *Creb1* decreased in PCM co-cultured with hSOD1(G93A) PCM confirming their ability to secrete miR-882 and -134-5p, the regulators of *Pax7* and *Creb1*, respectively (Figure 5B). On the contrary, we did not confirm a statistically significant downmodulation of *MyoD1* due to the upregulation of miR-882 induced by the secretion of hSOD1(G93A) PCM, although we observed a tendency toward *MyoD1* reduction concomitantly to miR-882 increase (Figure 5B). We tested the expression of other important targets of miR-26a-5p whose interaction with the miRNA had already been validated: *Smad1* and *Smad4*[38] (Figure S4). They are particularly important for skeletal muscle differentiation and regeneration,[39] and both were downmodulated in hSOD1(G93A) PCM co-cultured with hSOD1(WT) PCM (Figure 5B). All coding genes considered showed a negative correlation between their expression and that of regulatory miRNAs. This supports the functional relationship between miRNAs and the identified targets.

Secreted miRNAs from hSOD1(WT) PCM promote differentiation of hSOD1(G93A) myocytes by targeting SMAD pathway

Considering that miR-26a-5p-*Smad1*-*Smad4* interactions have already been validated[38] and that we demonstrated the upregulation of miR-26a-5p and the downmodulation of *Smad1* and *Smad4* in hSOD1(G93A) PCM co-cultured with hSOD1(WT) cells (Figures 5A and 5B), we tested if known targets of Smad4 TF were influenced

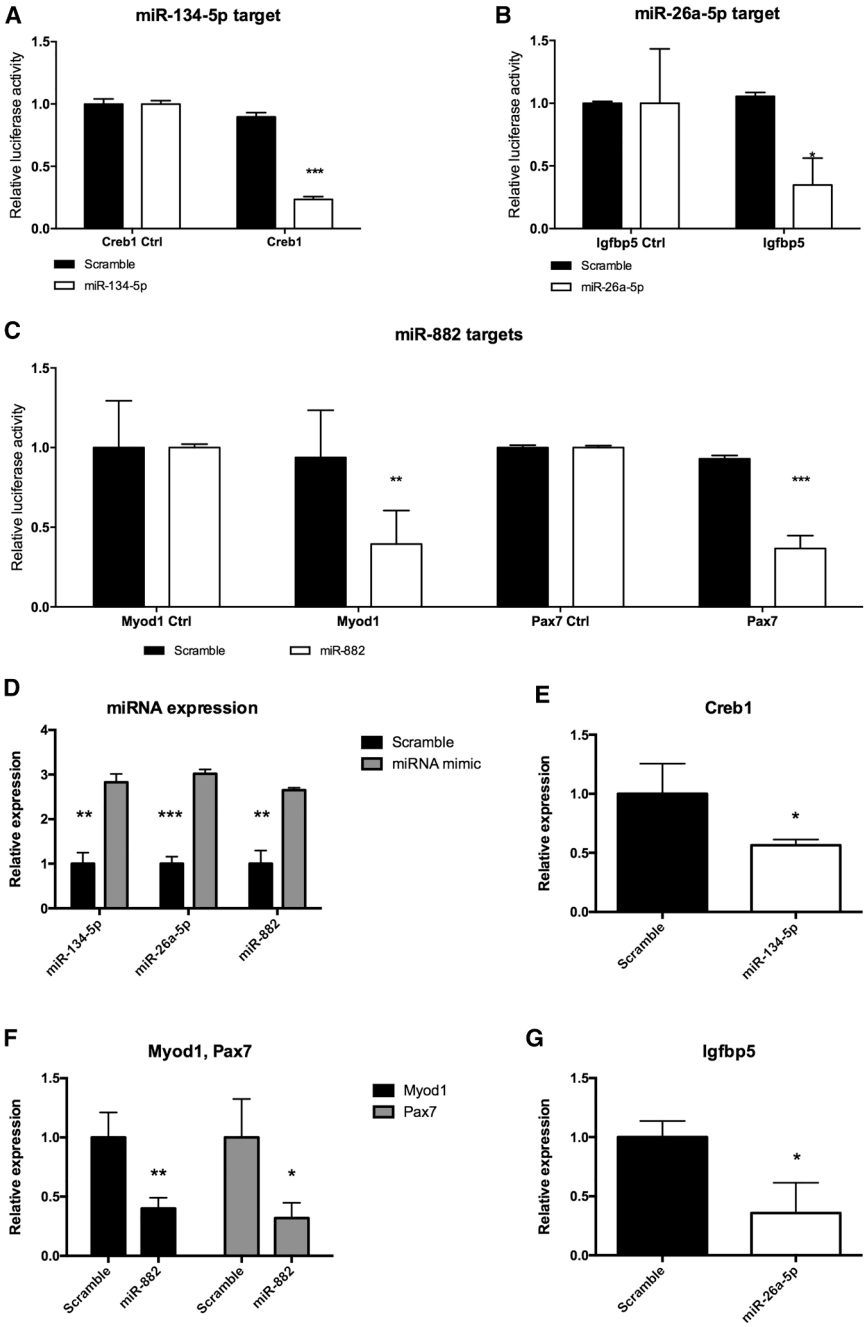

Figure 4. Luciferase reporter assay and miRNA activity in C2C12 cells

Luciferase reporter assays were performed to demonstrate the direct interaction between miRNAs and their targets. Part of the 3′-UTR sequence containing the miRNA putative interaction site (or not containing; Ctrl) was cloned in pmirGLO vector. Firefly luciferase (reporter gene) and Renilla luciferase (control reporter for normalization) activities were measured after the transfection in C2C12 cells together with miRNA mimics or miRNA scramble sequence (scramble). (A–C) Targets of miR-134-5p (A), miR-26a-5p (B), and miR-882 (C) showed a decreased luciferase activity. (D) After cell culture for 24 h with the medium containing miRNA mimics and 24 h of recovery, miRNAs within the cells increased their expression more than two times in comparison with the cells cultured with scramble sequence. Expression of miRNA targets validated by luciferase reporter assays decreased when the expression of miRNAs increased. (E–G) The expression of *Creb1* decreased about twice (E), *MyoD1* and *Pax7* by about 50 percent (F), and *Igfbp5* showed a decrease in its expression by one-third (G). Data are expressed as the mean of at least four independent transfections. Error bars indicate SD. *p* values from t tests considering independent variance between two groups in analysis are indicated as follows: $^{*}p < 0.05$, $^{**}p < 0.001$, and $^{***}p < 0.0001$.

by its downregulation in the same type of co-culture. Interestingly, the expression of three Smad4 targets (inhibitor of DNA binding 1 [Id1], leucine-rich repeat-containing G protein-coupled receptor 5 [*Lgr5*], and kinesin family member 7 [*Kif7*]) was diminished in hSOD1(G93A) PCM co-cultured with WT counterpart (Figure 5C). The effect of gene downmodulation we showed in Figure 5C can be indirect. Therefore, we next investigated Smad4 promoter occupancy on target genes by chromatin immunoprecipitation (ChIP)-PCR assay and found overall decreased enrichment associated with miR-26a-5p upregulation in hSOD1(G93A) PCM co-cultured with hSOD1(WT) cells (Figure 5D).

Myoblast secreted miRNAs influence motor neuron differentiation: miR-26a enhances neurite growth

We assessed the impact of secreted molecules from myoblasts on MN differentiation by employing conditioned media derived from hSOD1(WT) or hSOD1(G93A) myoblasts in MN differentiation media. This analysis demonstrated that the genotype hSOD1(G93A) exerts a detrimental effect on neurite development (Figures 6A and 6B). This result provides evidence that secreted miRNAs from myoblasts can also influence MNs. Given the significance of miR-26a in myoblast differentiation, we investigated the impact of its upregulation in MNs. Our findings revealed that this miRNA modulation can induce neurite length (Figures 6C and 6D). We utilized growth media derived from myoblasts stably expressing miR-26a, -134, and -431 to demonstrate that miRNAs secreted from the same myoblasts also influence MNs in a heterologous cell communication system. The medium derived from these myoblasts contained elevated levels of miRNAs that were upregulated (Figure S5). We demonstrated that the medium derived from myoblasts overexpressing miR-26a induced superior MN differentiation (neurite length exceeding

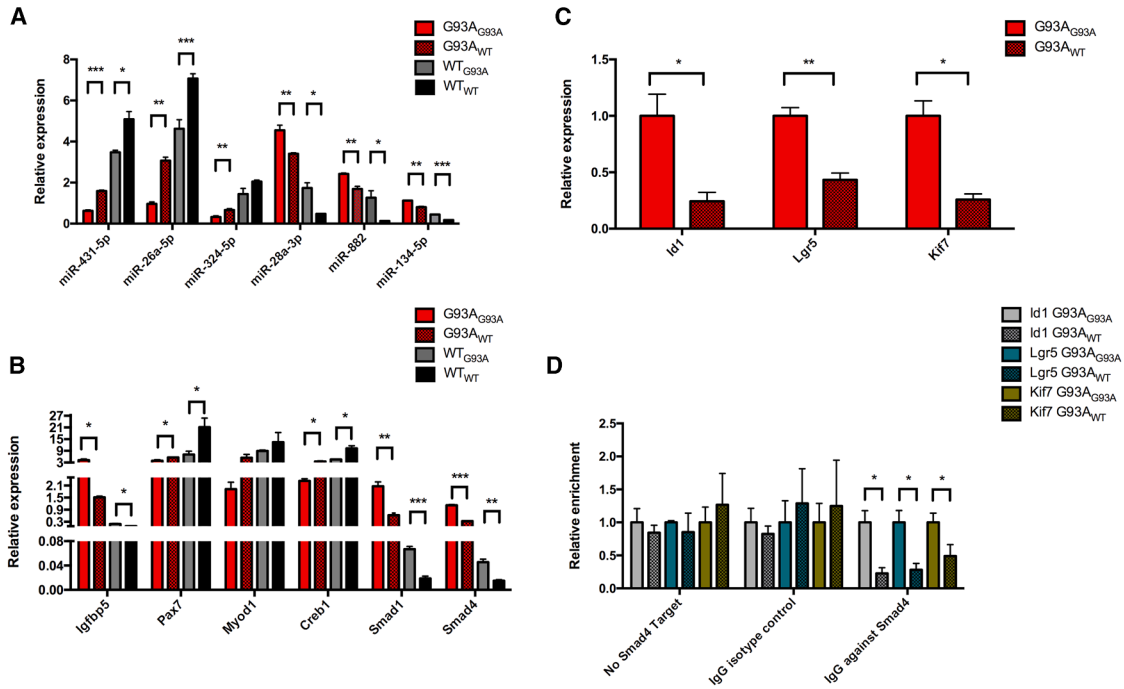

Figure 5. Relative expression of miRNAs and targets within hSOD1(G93A) or hSOD1(WT) myoblasts co-cultured with hSOD1(WT) or hSOD1(G93A) myoblasts respectively and Smad activity

(A) The bar diagram reports the normalized amount of miRNAs belonging to the blue (first three miRNAs) or violet (last three miRNAs) clusters in hSOD1(G93A) ($G93A_{G93A}$ or $G93A_{WT}$) or hSOD1(WT) (WT_{G93A} or WT_{WT}) cells co-cultured as reported in Figure S2. miR-26a-5p is the most expressed miRNA in hSOD1(WT) cells, while miR-28a-3p is most expressed in hSOD1(G93A) cells. (B) The bar diagram reports the normalized amount of miRNA targets. The expression of *Igfbp5* is decreased in $G93A_{WT}$ condition, while *Pax7*, *MyoD1*, and *Creb1* are more expressed both in the $G93A_{WT}$ and WT_{WT}. *Smad1* and *Smad4* show an opposite behavior respect to *Pax7*, *MyoD1*, and *Creb1*. Specular expression of miRNA and their targets support miRNA activity. (C) The bar diagram reports the normalized amount of Smad4 target genes in hSOD1(G93A) PCM co-cultured with hSOD1(G93A) PCM ($G93A_{G93A}$) or hSOD1(WT) ($G93A_{WT}$). Expression of all Smad4 target genes decreased in hSOD1(G93A) PCM co-cultured with hSOD1(WT) PCM. hSOD1(WT) PCM secrete miR-26a-5p that modulate the expression of *Smad4*. (D) Relative DNA enrichment after Smad4 chromatin immunoprecipitation. Considering a DNA region not associated with Smad4 interaction and the immunoprecipitation with the isotype antibody, no differences were evidenced between $G93A_{G93A}$ and $G93A_{WT}$ co-cultures. We obtained opposite and expected results after the utilization of IgG against Smad4 confirming the low abundance of Smad4 caused by the upregulation of miR-26a-5p. $^{*}p < 0.05$ and $^{**}p < 0.005$, calculated according to t test between indicated samples considering unequal variance. SD is indicated considering at least four replicates per experiment.

controls) with a phenotype compatible to that observed from the sole upregulation of this miRNA in MN (Figures 6E and 6F). This finding supports the hypothesis that miR-26a, secreted from myoblasts, is responsible for the observed MN phenotype. Similarly to miR-26a, miR-431 was found to be more abundant in the medium of hSOD1(WT) (Figure 5A). Notably, the medium produced by myoblasts overexpressing miR-431 exhibited an augmentation of the length of developing neurites (Figures 6E and 6F). In contrast, medium derived from myoblasts overexpressing miR-134, which we tested for its relevance to neuron function and synaptic plasticity such as miR-431,[40–42] did not exhibit significant effects on neurites of differentiating motor neuronal cells (Figures 6E and 6F). Notably, MN cells overexpressing miR-26a (Figure 6G) and those cultured in medium derived from C2C12 cells overexpressing miR-26a (Figure 6H) exhibit increased dendrite density per cell (Figure 6I), suggesting a role for miR-26a in MN differentiation. Furthermore, dendrites exhibit a branched structure when miR-26a is present (Figures 6G and 6H). This phenomenon is believed to enhance neural circuit complexity by facilitating interactions with a substantial number of targets.

The expression of miR-26a, Smad1, and Smad4 is consistently altered in SOD1(G93A) skeletal muscle

To unravel if the proposed mechanisms are detectable *in vivo*, we tested the expression of miRNAs in skeletal muscle samples from hSOD1(G93A) and hSOD1(WT) mice. Almost all miRNAs described in the Figure 3A were differentially expressed in at least one condition (Figures 7A–7C and S6). The expression of miR-882 was the only that did not result statistically different between WT and G93A but showed a progressive decrease with aging both in WT and G93A (Figure S6). Comparing results obtained with PCM, only the expression of miR-26a-5p was as expected (less abundant in hSOD1(G93A) genotype). Since we demonstrated that the expression and activity of *Smad1* and *Smad4* are regulated by

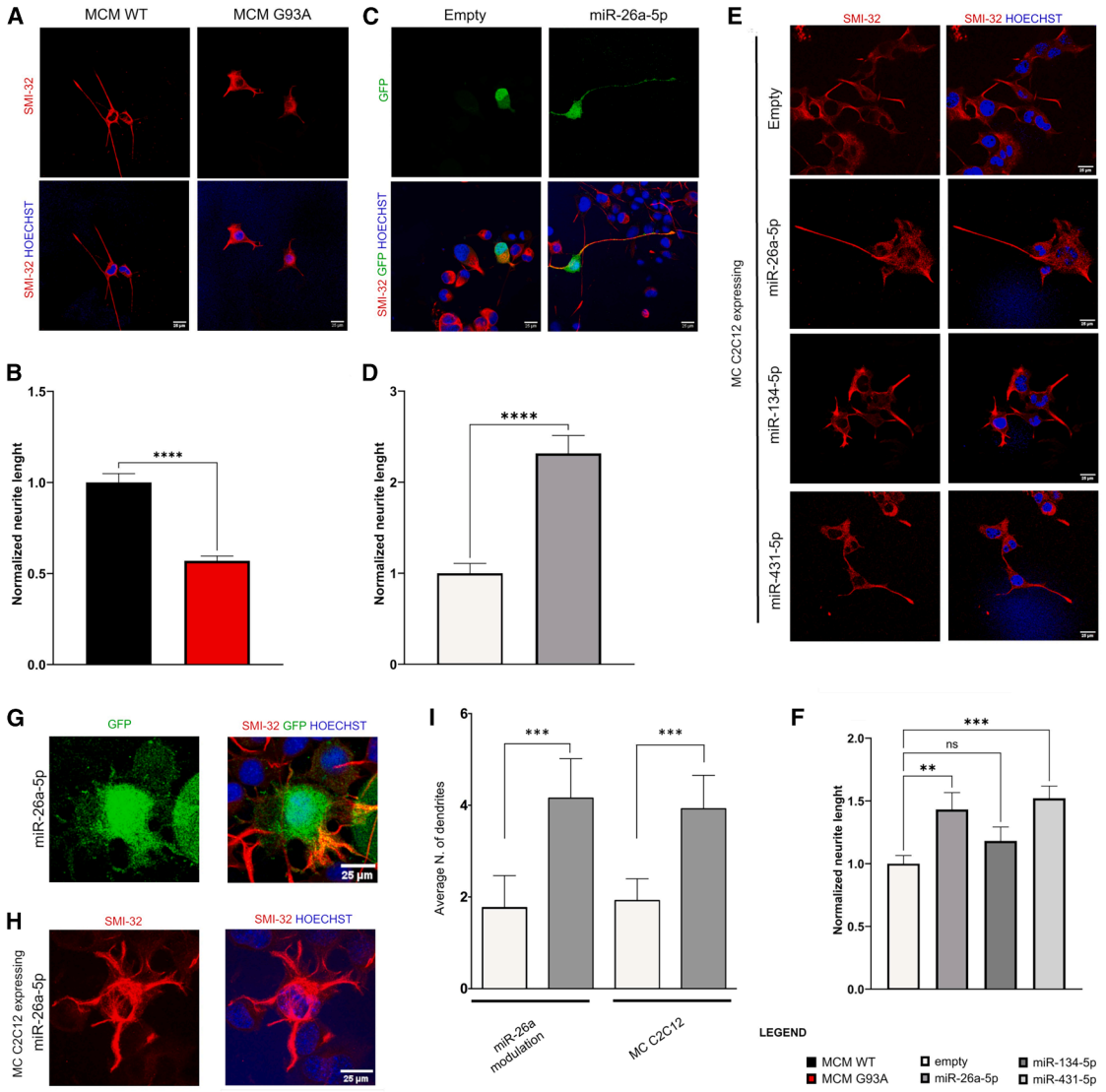

Figure 6. Activity of miRNAs on motor neuron cells

(A) Representative immunohistochemical images of motor neuron cultured with hSOD1(WT) (MCM WT) or hSOD1(G93A) PCM (MCM G93A). In blue, it is indicated cell nuclei and in red, motor neuron body and dendrites. (B) Calculation of neurite length. It decreases when hSOD1(G93A) PCM-derived culture medium was added to motor neurons. (C) Representative immunohistochemical images of motor neuron cells transfected with an empty pCMVmiR-GFP vector (empty) or a pCMVmiR-26a-GFP vector (miR-26a-5p) are presented. Green indicates transfected cells (GFP positive), blue indicates nuclei, and red represents the motor neuron body and neurites. (D) Only transfected cells (GFP-positive) were analyzed for neurite length, demonstrating an increase in neurite length when miR-26a is overexpressed. (E) Representative immunohistochemical images of motor neurons cultured in medium derived from C2C12 cells (MC C2C12) overexpressing miR-26a-5p, miR-134-5p, and miR-431-5p are presented. Red staining highlights the bodies and neurites of motor neurons, while blue staining depicts their nuclei. (F) Quantitative assessment of neurite length in motor neurons treated with culture medium derived from C2C12 cells overexpressing miR-26a-5p, miR-134-5p, and miR-431-5p. The miR-26a-5p and miR-431-5p miRNAs exhibit a stimulatory effect on neurite elongation. (G) Representative image of motor neuron neurite branching after miR-26a-5p overexpression. (H) Representative image of motor neuron neurite branching of motor neurons cultured in medium derived from C2C12 cells (MC C2C12) overexpressing miR-26a-5p. In both cases neurites appeared branched and several neurites outgrowth from cell body. (I) Quantification of neurites per body cell. The average number of neurites per 20 cells is represented. It increases when miR-26a is expressed from the cells (miR-26a modulation) or is present in the medium derived from C2C12 overexpressing miR-26a (MC C2C12). $^{**}p < 0.005$ and $^{***}p < 0.0005$, calculated according to t test between indicated samples considering unequal variance. SD is indicated considering at least three biological replicates and 15 cells analyzed per biological replicate.

miR-26a-5p, we evaluated the expression of the two TFs in the skeletal muscle during ALS progression. We showed that both *Smad1* and *Smad4* were downregulated in muscles of 3-month-old hSOD1(WT) mice (Figures 7D and 7E) when miR-26a-5p is upregulated.

The expressions of miR-26a-5p, -134-5p, -431-5p, Smad1, and Smad4 are altered in FUS skeletal muscle

To assess whether alterations observed in skeletal muscle samples from hSOD1(G93A) mice were genotype-specific, we analyzed the expressions of three miRNAs (miR-26a-5p, -134-5p, and -431-5p) in three different muscle types from FUS mice. We chose miR-26a-5p due to its pivotal role in the communication between myocytes and MNs, miR-134-5p, and miR-431-5p as they are crucial for neuron function and synaptic plasticity.[40–42] miR-26a-5p expression was upregulated in control muscle tissue from 4-week-old mice compared to those derived from FUS mice in both muscles enriched in fast myofibers (tibialis anterior [TA] and gastrocnemius [GAS]). Conversely, considering the same age, miR-26a-5p was not differentially expressed in the triceps, which contains a higher proportion of slow myofibers. Despite this, it exhibits a comparable trend at three weeks to the expression revealed in GAS and TA (Figure 7F). The expression of miR-431-5p exhibits a pattern similar to miR-26a-5p, with its upregulation in the control group compared to FUS in GAS and TA at four weeks. Notably, miR-431-5p is also upregulated in the control group in the triceps at three months, coinciding with the upregulating tendency of miR-26a-5p in the same region (Figure 7G). Results for miR-134-5p were more complex with any alteration in GAS and similar trend at three weeks in TA and triceps (Figure 7H). *Smad1* and *Smad4* were tested because we previously demonstrated that they are targeted by miR-26a-5p. We tested their expression in GAS derived from 4-week-old mice to compare results obtained from GAS from hSOD1(G93A) mice and to evaluate its correlation with the expression of miR-26a-5p in FUS mice. Both Smad1 and Smad4 were downregulated in WT GAS compared to FUS, where we had previously demonstrated the upregulation of miR-26a-5p (Figure 7I).

DISCUSSION

ALS is a neurodegenerative disease that affects the motor system. However, different cell types are affected: MNs are the most affected cells, but glial and skeletal muscle cells are also heavily involved and able to profoundly modulate the onset and progression of the disease. This complex interaction between MNs and neighboring and target cells makes it difficult to discover the exact pathological mechanisms that cause the progressive loss of MNs. Analysis of chimeric mice indicated that the restricted expression of human mutant SOD1 in MNs is not sufficient to induce a cell-autonomous degeneration of MNs.[43] This makes it important to study the involvement of other cells besides MNs in the development and progression of the disease. Direct muscle toxicity and/or functional impairment resulting in denervation and MN death has been demonstrated, at least in fALS[44–46] and muscle dysfunction and NMJ degeneration occur long before disease onset.[47] It was also demonstrated that skeletal muscle damage may in turn promote MN demise, in particular in SOD1-related ALS forms, as a consequence of dying-back mechanisms.[19] Moreover, very recently, it has been demonstrated that skeletal muscle contributes to the ALS phenotype also in C9orf72-related cases.[48] Finally, satellite cells also contribute to the initiation and progresison of ALS muscle atrophy.[22,24] Data presented in this paper corroborate previous reports describing skeletal muscle damages in ALS and impaired myogenesis in different primary and immortalized myocyte models of ALS (for a review, see study by Peggion et al.[12]). We have identified the potential for satellite cells/myocytes to exhibit altered communication patterns even in a preclinical condition via secreted miRNAs. We evidenced the contribution of miRNAs in the expression regulation of important genes coding for proteins involved in myogenesis. These miRNAs can exacerbate pathological condition or ameliorate differentiation potentiality of myocytes derived from the hSOD1(G93A) ALS mouse model. Furthermore, the same miRNAs that facilitate myoblast differentiation also influence MN differentiation, maintaining a continuous communication between myocytes and MNs.

Myogenesis is a highly complex, finely regulated process,[49] whose alteration impacts muscle regeneration.[50] Therefore, to explore the possibility that altered myogenesis is an intrinsic defect in ALS early stages rather than a simple consequence of MN loss, we set up primary myocyte cultures from hSOD1(G93A) and control pups. We showed a delayed *in vitro* differentiation of hSOD1(G93A) primary myocytes, as demonstrated by the altered expression of several skeletal muscle differentiation markers.

In particular, we found a reduced expression of Pax7, a key player in the prenatal and postnatal myogenesis processes, that belongs to the Pax gene family that is critical for satellite cell biogenesis, survival, and self-renewal.[51] Moreover, we also found an altered expression of MyoD and myogenin, both belonging to the MRF family that act as an orchestrating cascade in proliferation, induction of terminal cell-cycle arrest, and stimulation of the differentiation process.[51] Such results confirm previous data demonstrating a reduced expression of Pax7 and MyoD in skeletal muscle biopsies from ALS patients[52] and of myogenin in quadriceps derived from adult hSOD (G93A) Tg mice.[45] They also demonstrate that skeletal muscle precursor cells from newborn mice (showing no pathologic phenotype) display molecular alterations that are responsible for the phenotypic manifestations of pathology in adult muscle.

The expression of TFs during myogenesis is finely regulated by the activation of different signaling cascades, mainly controlled by protein kinases, which transmit and execute extracellular promyogenic cues. Here, we showed an impaired activation of p38 MAPK in ALS primary myocytes. The p38 pathway plays a critical role in the regulation of myogenesis and muscle cell differentiation, by acting at multiple levels and through many distinct mechanisms.[53] For example, p38 phosphorylates several MRFs during skeletal muscle differentiation, enhancing the expression of MyoD-responsive genes and the transcriptional activities of myocyte enhancer binding

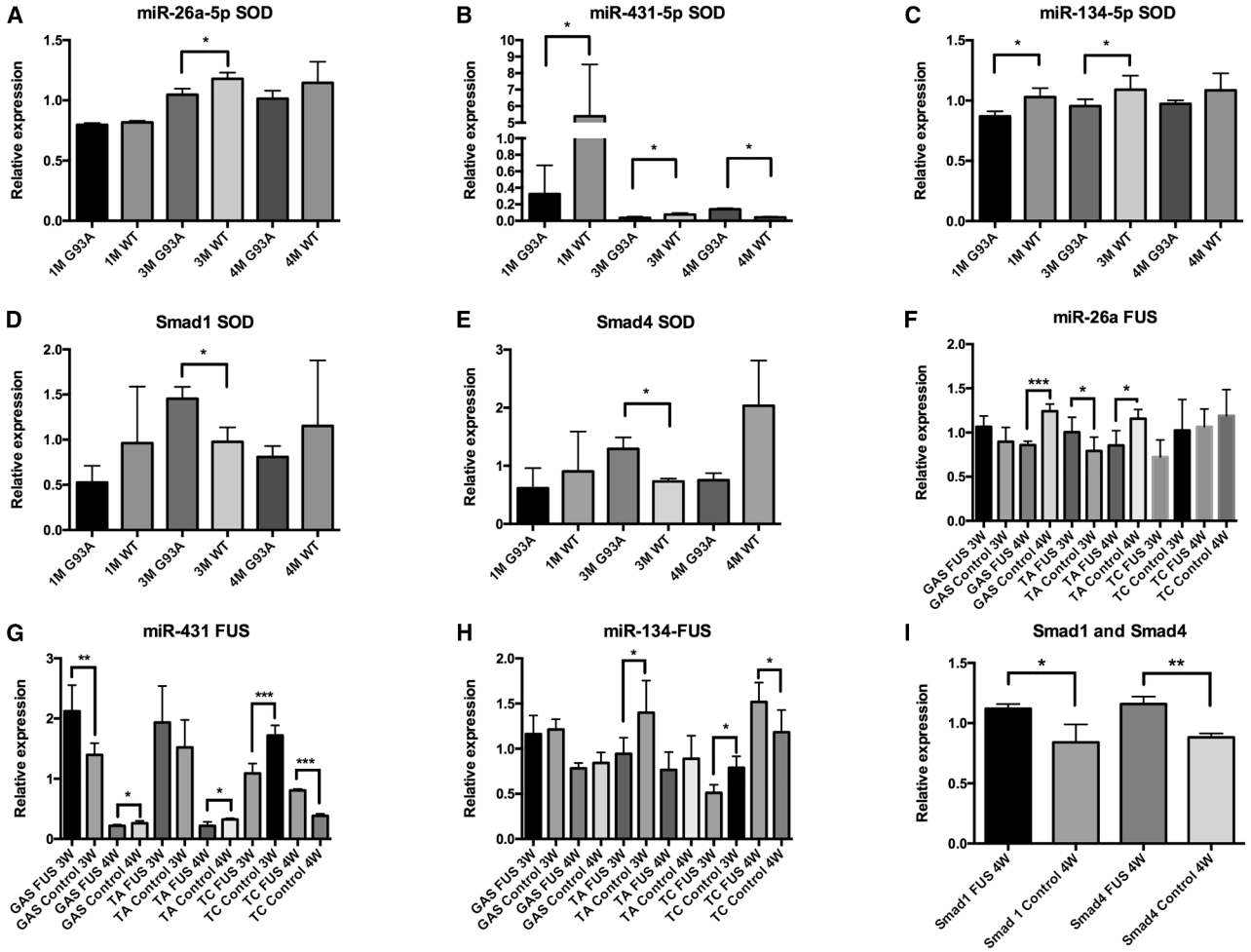

Figure 7. Gene expression of miRNAs and Smad1 and Smad4 in skeletal muscle

(A–E) SOD1 mouse model. Expression relative to the average expression of the gene in all samples. 1M, 3M, and 4M indicate 1 month, 3 months, and 4 months, respectively. Analyses were conducted on three biological replicates and four technical replicates for each sample. (F–I) FUS mouse model. 3W and 4W indicate 3 weeks and 4 weeks. GAS, gastrocnemius; TA, tibialis anterior; TC, triceps; F, FUS mouse; C, control. Analyses were conducted on three biological replicates and two technical replicates for each sample. *$p < 0.05$, according to Mann-Whitney test.

factors 2A (MEF2A) and MEF2C by direct phosphorylation.[54] The various functions attributed to p38 in myogenesis also include the control of myoblast fusion and myofiber formation through the up-regulation of CD53[55] and the increased expression of p21 and myogenin.[56] Interestingly, our data demonstrated a reduced expression of both p21 and myogenin. Our findings support a reduced activation of the p38/MyoD and p21 axes and suggest that the impairment of such a signaling pathway is strictly related to defective skeletal muscle differentiation and—possibly—regeneration in ALS.

Our data also showed alterations in the PKA signaling pathway, as evident from the reduced phosphorylation (activation) of its substrate CREB. Among other cell functions, this TF is involved in myoblast proliferation and differentiation *in vitro* and proliferation and muscle regeneration *in vivo*[57] through its ability to act in the Wnt-mediated transcription of myogenic TFs such as Myf5, MyoD, and Pax3.[35]

Starting from our findings of defective myogenesis in hSOD1(G93A) PCM, and the phenotypic rescue operated by the presence of control/healthy PCM, we searched for secreted miRNAs that may be involved in described processes by large-scale analyses. It is well known that the skeletal muscle acts as a secretory organ by producing cytokines (e.g., insulin-like growth factor [IGF]-1 and tumor necrosis factor alpha) and other fiber-derived molecules, which have autocrine and paracrine effects on skeletal muscle precursor cell proliferation and muscle hypertrophy[58,59] and also regulate a variety of other metabolic processes.[60–62] Soluble secreted factors or alterations of extracellular molecules may in addition be markers of intrinsic skeletal muscle alterations. Importantly, the composition and relative

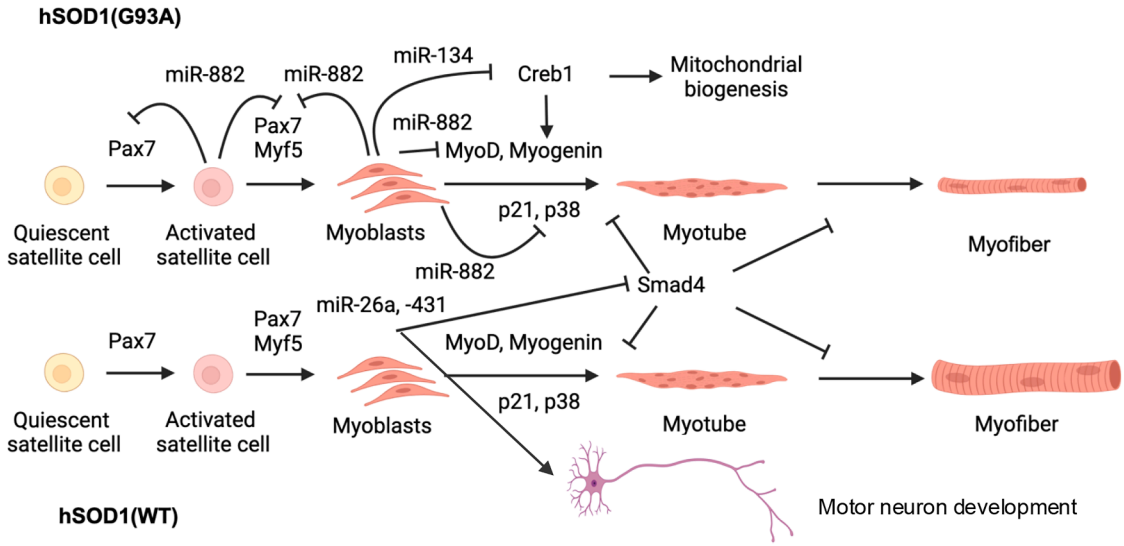

Figure 8. Schematic description of proposed mechanisms

The downmodulation of significant MRFs prevents the proper differentiation of hSOD1(G93A) myocytes. Particularly, miR-882 and -134-5p downmodulate *Pax7*, *MyoD*, *Creb*, and *p38*. hSOD1(WT) PCM secretes miR-26a-5p that impacts on the expression and functionality of *Smad4*. It inhibits muscle differentiation; therefore, its downmodulation may stimulate muscle differentiation. miR-26a, in concert with miR-431, affects the differentiation of motor neuron by increasing the legth of their neurites..

abundance of skeletal muscle secretome strictly depends on the myocyte differentiation stage.[63] Alteration in several secreted cytokines and peptide hormones have been already associated to skeletal muscle in ALS.[45,64–66] In addition, the alteration of metabolites secreted by hSOD1(G93A) PCM has already been demonstrated.[30]

It was already known that alterations in the expression of miRNAs are related to ALS[67] and also to other neuro-muscular diseases and myopathies.[68]

However, here, for the first time to our knowledge, we specifically evaluated secreted miRNAs from satellite cells from hSOD1(G93A) muscle and differences in miRNA secretion of the same cells respect to hSOD1(WT) muscle. Furthermore, we elucidated the mechanisms by which specific miRNAs maintain impaired differentiation in hSOD1(G93A) PCM. Additionally, we demonstrated that these miRNAs can rescue this phenotype, thereby highlighting the miRNA-mediated influence of myocytes not only on their differentiation but also for that of MNs (Figure 8). miRNAs secretion and transfer to other cells occurs via vesicles[69] or prevalently by protein association.[70] Since methods to purify exosomes allow to recover only a subpopulation of secreted miRNAs, we purified secreted miRNAs by avoiding any step of exosome purification. We identified 492 secreted miRNAs and 53 of them resulted differently concentrated in one of the conditions analyzed. Among different altered miRNAs we confirmed the expression of six of them by RT-qPCR: miR-431-5p, -26a-5p, and -324-5p less abundant in the culture medium of hSOD1(G93A) and miR-28a-3p, -882, and -143-5p more abundant in the culture medium of the same myocytes. Considering differentiation ability of each genotype, we can define permissive as the most abundant miRNAs in the co-culture composed only of hSOD1(WT) PCM and non-permissive as the most abundant miRNAs in the co-culture composed only of hSOD1(G93) PCM.

miR-26a and -431 are involved in skeletal muscle and neuron differentiation, regeneration, and maintenance.[38,40,71–75] miR-26a, in particular, plays a role in promoting myoblast differentiation and is required for skeletal muscle regeneration after injury by targeting *Smad1* and *Smad4*.[38] Moreover, miR-26a inhibits neuropathic pain development.[76] These notions suggest that manipulating miR-26a levels may have therapeutic potential for treating skeletal muscle diseases to prevent muscle wasting and neuropathic pathologies. We showed how this miRNA can be secreted by WT cells and taken up by hSOD1(G93A) cells where, by regulating *Smad4*, it interferes with the regulation of specific targets of the TF itself by decreasing its occupancy of promoter binding sites. We showed that miR-26a-5p also regulates insulin-like growth factor binding protein-5 (*Igfbp5*), an important modulator of the IGF signaling. *Igfbp5* is the most conserved across species[77] and plays an important role in development and biological processes of muscle.[78] Interestingly, the overexpression of *Igfbp5* in mice caused a severe body growth reduction both prenatally and postnatally, and a 30% reduction in skeletal muscle weight.[79] Additionally, we demonstrated that miR-26a, secreted from myoblasts, facilitates the elongation of neurites in developing MN cells, thereby supporting the notion of intercellular communication. miR-26a-5p is downmodulated in the muscle of both SOD1(G93A) and FUS mice while its targets (*Smad1* and *Smad4*) are increased in their expression. This may impact muscle regeneration also in association to a possible expression of Igfbp5 permitted by miR-26a-5p downmodulation. Notably, the similar

expression of miR-26a-5p, *Smad1*, and *Samd4* between SOD1 (G93A) and FUS mice suggests that the proposed mechanism may be applicable to various ALS models, not only to the one based on the SOD1 G93A mutation.

miR-431 also promotes muscle regeneration by targeting *Smad4* and fine-tuning *Pax7* levels.[72] It also plays a role in the regulation of axon regeneration.[80] We have shown that it is secreted by WT myocytes and uptaken from hSOD1(G93A) and MNs probably sustaining the action of the miR-26a. Recently, it was reported that miR-324-5p inhibits C2C12 cell differentiation and promotes intramuscular lipid deposition via the inhibition of the long non-coding RNA lncDum.[81] However, the same study shows that the expression of miR-324-5p increases during the first four days of C2C12 differentiation demonstrating its importance in the first phases of differentiation. In fact, miR-324 upregulation promotes differentiation of human primary myocytes.[82]

Among miRNAs secreted from hSOD1(G93A) PCM, miR-28a, although poorly studied in the skeletal muscle, was reported to be upregulated during human myoblast differentiation[82] and downregulated in muscle and serum/plasma after exercise.[83] These last results support detrimental activity of miR-28a in skeletal muscle. We evidenced that it is upregulated in hSOD1(G93A) PCM and it is known that exercise, that induces its downregulation in muscle, has beneficial effects on health, also promoting the activation of muscle repair pathways. miR-28a was also studied in cardiac muscle, where its reduction ameliorates oxidative stress induced apoptosis.[84] We report here that miR-28a expression is reduced in the skeletal muscle of hSOD1(G93A) 4-month-old mice, when inefficient antioxidant defense represents an important pathological feature.

There is limited specific information available regarding the role of miR-882 in muscle function. We showed its centrality in the myogenic network through its ability to regulate the expression of *MyoD1* and *Pax7* that are downexpressed in hSOD1(G93A) PCM (Figure 8). miR-882 is more secreted by hSOD1(G93A) PCM, suggesting its upregulation in the same cells that may cause downregulation of *MyoD1* and *Pax7*. Analysis of miR-882 expression in the muscle of SOD1(G93A) mice did not show significant differences with their respective controls but highlighted progressive downregulation over time. Probably, this different expression of miRNAs in skeletal muscle and PCM can be explained by the complexity of skeletal muscle, where most of the cells are myofibers or fibroblasts, in the case of degeneration, and not satellite cells, that are the main focus of this study.

The expression of miR-134-5p was studied during post-natal mouse skeletal muscle development.[85] It is particularly expressed two days after birth, and then its expression decreases until it reaches its minimum after 12 weeks after birth. Therefore, miR-134-5p is important in the first stages of post-natal muscle differentiation. miR-134-5p enhances differentiation in embryonic stem cells[86] and also impacts on differentiation of neuronal progenitor cells.[87] We confirmed its interaction with *Creb1* and added another piece to the puzzle in the regulation of the PKA signaling pathway (Figure 8). miR-134 also localizes to dendrites, where it influences dendritic spine morphology.[41] Furthermore, the induction of miR-134, along with other miRNAs from the miR-379–410 cluster (miR-381 and miR-329), is essential for activity-dependent dendritogenesis in primary hippocampal neurons.[88] We showed that culture medium from myoblasts overexpressing miR-134 did not impact MN morphology and neurite length.

Conclusions

This work demonstrates that skeletal muscle precursor of neonatal hSOD1(G93A) mice are different from those derived from hSOD1 (WT), supporting the idea that even satellite cells in a pre-phenotypic condition retain molecular alterations associated with ALS. In addition, the possibility of communication between different types of myocytes and MNs has been elucidated. This observation makes it possible to think about cell therapy based on overexpression of molecules that can be secreted to improve the phenotype of defective cells or the differentiation ability of satellite cells. We showed that satellite cells secrete a plethora of miRNAs that have a positive or negative impact on their differentiation in relation to the genotype of secreting cells. Considering the therapeutic opportunity, we highlighted the importance of hSOD1(WT) myocytes in secreting miR-26a, which, when assimilated by hSOD1(G93A) myocytes, enables better differentiation by targeting *Smad4* and limiting the induction of Smad4-regulated genes. Furthermore, miR-26a, in conjunction with miR-431, both of which are upregulated in hSOD1(WT) myocytes, influences MN differentiation, thereby extending the length of the neurites produced. This supports the importance of miRNAs in modulating intercellular communication and the possibility of using them to regulate skeletal muscle differentiation even in a genetically inherited pathological condition.

MATERIALS AND METHODS

Mouse models

Tg mice overexpressing WT hSOD1 protein (strain B6SJL(Tg-SOD1)2Gur/J), here abbreviated as hSOD1(WT), or the G93A mutant form (B6SJL(Tg-SOD1*G93A)1Gur/J), here abbreviated as hSOD1(G93A), were from Jackson Laboratories (cat. nos. 002297 and 002726, respectively). Colonies were preserved by breeding Tg hemizygote males with WT B6SJLF1/J hybrid females. Newborns were genotyped as previously described[89] using the MyTaq Extract-PCR kit (Bioline). For the skeletal muscle analyses, mice (1, 3, and 4 months old) were sacrificed by cervical dislocation.

Tg mice overexpressing WT hFUS protein (Tg(Prnp-FUS) WT3Cshw/J), here abbreviated as FUS mice, were from The Jackson Laboratory (cat. no. 017916). These mice were maintained as hemizygotes on a C57BL/6 genetic background. Genotyping of newborn mice was performed by standard PCR on DNA extracted from phalanx biopsies, using primer sets provided by The Jackson Laboratory. Hemizygous FUS mice were backcrossed to obtain homozygous animals, whose skeletal muscles were analyzed at the presymptomatic

(3 weeks of age) and onset (4 weeks of age) stages of the disease. For tissue collection, animals were deeply anesthetized via intraperitoneal injection of ketamine hydrochloride (IMALGENE, 100 mg/kg; Alcyon Italia) and medetomidine hydrochloride (DOMITOR, 1 mg/kg; Alcyon Italia), and subsequently sacrificed by decapitation.

Primary myocyte cultures

Primary myoblasts from newborn (1–3 days) hSOD1(WT) or hSOD1(G93A) mice were prepared as previously described.[90] Briefly, the posterior limb muscles were removed, and cells isolated by three successive treatments with 0.1% trypsin in phosphate-buffered saline (PBS; 140 mM NaCl, 2 mM KCl, 1.5 mM KH_2PO_4, 8 mM Na_2HPO_4 [pH 7.4]) for 30 min at 37°C, seeded at a density of 2.5×10^5 cells onto 13-mm coverslips coated with collagen (0.1% w/v in PBS) for immunocytochemistry, or at a density of 1×10^6 cells onto 35-mm collagen-coated plates for biochemical assays, and cultured in proliferation medium (Ham's F12 with 10% fetal bovine serum [FBS], 2 mM glutamine, 100 U/mL penicillin, and 100 μg/mL streptomycin) for 2 days (2 DIV). At this time point, proliferation medium was replaced by differentiation medium (Dulbecco's modified Eagle's medium containing 2% horse serum, 2 mM glutamine, 100 U/mL penicillin, and 100 μg/mL streptomycin) for myoblast differentiation into myotubes. All reagents for cell culture were from Euroclone.

NSC-34 motor neuron culture and differentiation

The NSC-34 MN cell line[91] as maintained in growth medium consisting of DMEM supplemented with 10% FBS, 4 mM L-glutamine (Gibco), and 100 U/mL penicillin/100 μg/mL streptomycin (Gibco). To induce differentiation, the cell cultures were switched to differentiation medium consisting of Neurobasal (Gibco), 4 mM L-glutamine (Gibco), and 100 U/mL penicillin/100 μg/mL streptomycin (Gibco).

For the NSC-34 neurite growth assay, cells were seeded in triplicate onto collagen I (Enzo ALX-522-440-0050)-coated coverslips at a density of 4,000 cells/cm^2 in 400 μL. Cells were incubated with different mediums for 48 h: (1) differentiation medium alone (controls); (2) 50% MCM (primary myoblast conditioned medium) and 50% differentiation medium; and (3) 50% of the medium from C2C12 cells overexpressing miR-26a, -134a, or -431 and 50% of differentiation medium.

Preparation of co-cultures of myocytes and conditioned medium

Co-culturing experiments were carried out in 24-well transwell plates (tw) (Sarstedt) using four different cell combinations: (1) hSOD1(WT) myocytes cultured on the bottom chamber ("target cells") and on the insert ("donor cells") (WT_{WT}); (2) hSOD1 (G93A) and hSOD1(WT) myocytes cultured on the bottom chamber and the insert, respectively ($G93A_{WT}$); (3) hSOD1(G93A) myocytes cultured on the bottom chamber and on the insert ($G93A_{G93A}$); and (4) hSOD1(WT) and hSOD1(G93A) myocytes cultured on the bottom chamber and on the insert, respectively (WT_{G93A}) (Figure S2). Myoblasts were seeded in the collagen-treated upper insert (0.4 μm pore size) at the concentration of 1.5×10^5 cells and in the lower collagen-treated chamber at the concentration of 2.5×10^5 cells and cultured in proliferating media for 2 days and then in differentiation media. For both western blot (WB) and immunocytochemistry, cells on the bottom chamber of conditions (1), (2), and (3) were used. The myocytes for immunocytochemistry were grown on coverslips, while those for WB analysis were grown directly on the plastic of the bottom chamber.

For the preparation of MCM, the supernatant of well-tw chambers from the combinations (1), (2), and (3) of co-cultured cells was collected at 2 DIV, centrifuged at 16,000 × g (4°C, 5 min) to remove cell debris, and stored at −80°C for miRNA analyses.

In the co-culture conditions, miRNA functional studies were performed with cells cultured on the bottom well.

Immunocytochemistry

Four DIV primary cultures and differentiated NSC-34 cells grown on coverslips were rinsed twice with PBS and fixed with paraformaldehyde (2% (w/v) in PBS, 20 min, 4°C). After permeabilization in Triton X-100 (0.5% [w/v] in PBS, 15 min, room temperature [RT]), primary cultures were incubated (overnight, 4°C) with mouse monoclonal antibody anti-desmin (mAb) (Boehringer Mannheim, cat. no. 814377; 1:50 dilution in PBS containing 1% [w/v] bovine serum albumin [BSA], PBS-BSA). NSC-34 differentiated cells were stained with anti-neurofilament SMI32 (BioLegend, cat. no.801701; 1:200) diluted in PBS containing 1% (w/v) BSA, PBS-BSA. After extensive washings in PBS, cells were incubated (1 h, RT) with Alexa Fluor 555-conjugated anti-mouse IgG (Molecular Probes, Thermo Fisher Scientific, cat. no. A21424, 1:500 dilution in PBS-BSA), and finally counterstained with the Hoechst 33342 nuclear fluorogenic probe (Sigma-Aldrich, 5 μg/mL in PBS, 20 min, RT). After further washings in PBS, the coverslips were mounted onto microscope slides using a fluorescence mounting medium (DAKO). Myotubes were observed with an inverted fluorescence microscope (Axiovert 100, Zeiss) equipped with a computer-assisted charge coupled camera (AxioCam, Zeiss) at 10× magnification. Images from different fields were digitalized and stored for subsequent analysis, while MNs were observed using a Leica Stellaris 8 inverted confocal microscope.

Phenotypic characterization of myotubes and motor neurons

The stage of myogenic differentiation at 4 DIV was assessed by the following parameters.

(1) The differentiation index was calculated as the ratio between the sum of myonuclei and the total number of desmin-positive cells.
(2) The fusion index (FI) was calculated as the ratio between the number of total nuclei inside desmin-positive myotubes with more than three nuclei and the total number of myonuclei.

Counts for both FI and the differentiation index were performed in 16 randomly selected fields from four different biological

replicates and reported as mean ± SEM of four different cultures for each condition.

(3) Differentiated myotubes were recognized by desmin-positive staining and the presence of at least two nuclei. Myotube area was measured by the ImageJ software. For determining the area frequency distribution, myotubes with surface area between 0 and 100,000 or 150,000 pixels were split into twenty intervals of 5,000- or 7,500-pixel, respectively, and the frequency of myotubes in each interval was calculated.

To analyze neurite length of differentiated NSC-34 cells, images were obtained using a Leica Stellaris 8 inverted confocal microscope with laser illumination at 405, 488, and 555 nm wavelengths, depending on the fluorescent probes used, and an HC PL APO CS2 40×/1.30 oil-immersion objective. For all images, the pinhole was set to 1 Airy unit. Confocal microscopy imaging was performed at 1,024 × 1,024 pixels per image, with a 0.2 Hz acquisition rate. To avoid crosstalk between fluorophores, sequential scans (using the "between frames" option) were performed. Subsequently, a z stack was acquired through the entire thickness of the cell at 290 nm intervals in the *z*-plane. Analysis of neurite length was carried out using the NeuronJ program, a plug-in for the ImageJ analysis program. The number of dendrites originating from body cells was quantified in the MN cell line overexpressing miR-26a, as well as in those treated with the medium derived from C2C12 cells overexpressing the same miRNA.

Western blot analysis

After two washes with ice-cold PBS, PCM at different DIV were lysed in an ice-cold lysis buffer containing 10% (w/v) glycerol, 2% (w/v) SDS, 62.5 mM Tris/HCl (pH 6.8) and protease and phosphatase inhibitor cocktails, and then centrifuged (14,000 × g, 10 min, 4° C) to pellet cell debris. The total protein content in the supernatant was determined by the bicinchoninic acid assay kit (Thermo Fisher Scientific) according to the manufacturer's instructions. Protein samples were then diluted to the desired concentration by adding dithiothreitol (f.c., 50 mM) and bromophenol blue (f.c., 0.004% [w/v]), and boiled (5 min). Proteins were separated by SDS-PAGE using 7% or 10% (w/v) acrylamide-N,N′-methylenebisacrylamide (37.5:1 [w/w]) for the analysis of high or low molecular weight proteins, respectively, or Mini-Protean TGX pre-cast gels (4%–20%, Bio-Rad Laboratories), and then transferred onto polyvinylidene difluoride (PVDF) membranes (0.45 μm pore size; Bio-Rad Laboratories). Membranes were incubated in Tris-buffered saline (TBS, 20 mM Tris-HCl (pH 7.6) and 150 mM NaCl) added with 0.1% (w/v) Tween 20 (TBS-T) and 3% (w/v) BSA (Sigma-Aldrich) as blocking solution (1 h, RT), and then incubated with the desired primary Ab diluted in blocking solution (overnight, 4°C). After washing in TBS-T, membranes were incubated (1 h, RT) with horseradish peroxidase-conjugated anti-mouse or anti-rabbit (Sigma-Aldrich, cat. nos. A9044 and A0545, respectively) depending on the primary Ab used. After washing in TBS-T, immunoreactive bands were visualized and digitalized by means of a digital camera workstation (NineAlliance, UVITEC, Eppendorf), using an enhanced chemiluminescence reagent kit (Millipore). For densitometric analyses, the optical density of each immunoreactive band was normalized to the optical density of the corresponding Coomassie blue (50% [v/v] methanol, 7% [v/v] acid acetic, 0.01% [w/v])-stained lane.[92] For the analysis of phosphorylated proteins, samples were run in parallel onto different gels, and PVDF membranes were probed with antibodies recognizing either the phosphorylated or the total form of the protein of interest. Densitometric values of each phosphorylated protein were normalized to those of the corresponding total protein band (calculated as aforementioned).

The following primary Abs were used: anti-EmbMyHC mouse mAb (cl.BF-G6), 1:5,000 (Developmental Studies Hybridoma Bank, University of Iowa); anti-CREB rabbit mAb, 1:1,000 (Cell Signaling Technology, cat. no. 9197s); anti-pSer133 CREB mouse mAb, 1:1,000 (Cell Signaling Technology, cat. no. 9196s); anti-p38 rabbit polyclonal antibody (pAb), 1:1,000 (Cell Signaling Technology; cat. no. 9212); anti-pThr180/Tyr182 p38 rabbit mAb, 1:1,000 (Cell Signaling Technology; cat. no. 9211); anti-Pax7 mouse mAb, 1:300 (Santa Cruz Biotechnology, cat. no. sc-81648); anti-MyoD mouse mAb (cl. 5.8A), 1:1,000 (Thermo Fisher Scientific, cat. no. MA5-12902); anti-myogenin mouse mAb, 1:1,000 (Abcam, cat. no. Ab 1835); anti-Phospho-PKA substrate (RRXS*/T*) (100G7E) rabbit mAb, 1:500 (Cell Signaling Technology; cat. no. 9624); anti-Akt1/2/3 (H-136) pAb, 1:1,000 (Santa Cruz Biotechnology, cat. no. sc-8312); anti-pSer473-Akt1/2/3 rabbit pAb, 1:1,000 (Santa Cruz Biotechnology, cat. no. sc-7985-R); and anti-p21 (WAF1) mouse mAb, 1:250 (Merck, Calbiochem, cat. no. P1484).

RNA extraction

Secreted miRNAs in the MCM were extracted using the TRIzol LS solution (Thermo Fisher Scientific) following the manufacturer's protocol. Briefly, 600 μL of TRIzol LS (Thermo Fischer Scientific) were added to 200 μL of culture medium; after 5 min of incubation at RT, 160 μL of chloroform were added. After mixing, the solution was incubated on ice for 15 min and then centrifugated at 12,000 × g at 4°C for 20 min. Aqueous phase was transferred in a new tube and precipitated at −20°C overnight adding an isovolume of isopropanol. The RNA was washed two times with 80% of ethanol and resuspended in 10 μL of DNAse/RNAse free water (Thermo Fisher Scientific). For each condition, we extracted miRNAs three times from 200 μL of medium totally using about 600 μL of medium. RNA extracted from the same sample was pooled and the concentration of miRNAs was inferred according to the run in the 2100 Agilent bioanalyzer using the smallRNA chip (Agilent Technologies) and integrating the area under desired nucleotide dimension (18–26 nucleotides).

Total RNA from skeletal muscles (gastrocnemius for SOD1 mice and gastrocnemius, TA, and triceps for FUS mice) and C2C12 cells and PCM were extracted as we previously described in a study by Codolo et al.[93] following the TRIzol protocol.

Microarray expression profiles

Agilent Mouse miRNA Microarray 8 × 60 K platform (Agilent Technologies) was used to profile the expression of secreted miRNAs in three different conditions of co-culture: (1), (2), and (3) (see aforementioned text for the explanation of co-cultures). miRNAs (150 ng) (according to the concentration established by the 2100 Agilent bioanalyzer runs) were labeled using miRNA Complete Labeling and Hyb Kit (Agilent Technologies), according to the manufacturer's protocol. Labeled RNA was hybridized onto microarray slides using a rotational oven at 55°C for 22 h. At least three biological replicates were used for each condition (excluding the WT_{WT} co-culture that was screened with two biological replicates). After hybridization, miRNA microarray slides were washed using the Wash Buffer Kit (Agilent Technologies) and dried at RT. Microarray slides were scanned using a G2505C scanner (Agilent Technologies) at 3 μm resolution. Probes features were extracted using the Feature Extraction Software v. 10.7.3.1 with GE 1 Sep09 protocol (Agilent Technologies).

Microarray data analysis and identification of miRNA function

Raw microarray data were first filtered for the number of miRNAs presenting an expression value above the background (0% of undetected values per sample type were allowed for each miRNA) and then normalized according to the loess cyclic algorithm, as previously described.[94] Kruskal-Wallis Test was performed to identify differentially expressed miRNAs, using 0.05 as the *p* value cut-off. Pearson correlation with average linkage method was used to cluster miRNAs and samples. miRNA function was inferred according to the function of their targets. We decided to identify the function of miRNAs using miRTarBase (release 8) and TarBase 8.0[95,96] databases. Interactions between miRNAs and their targets were shown using the Cytoscape software (https://cytoscape.org/index.html). Edges among protein coding genes represent interactions retrieved from Biogrid database (*Mus musculus* 4.4.217) (https://thebiogrid.org/).

RT-qPCR experiments

TaqMan method was used to evaluate miRNA expression by RT-qPCR. Secreted miRNAs (2 ng) or total RNA (10 ng) (in the case of miRNAs within cells or tissues) were retrotranscribed using the TaqMan MicroRNA Reverse Transcription Kit (Thermo Fisher Scientific), according to the user manual. RT-qPCR was performed using the 7500 Real-Time PCR System (Thermo Fisher Scientific) in 20 μL using the Taq Man Universal PCR Master Mix II (Thermo Fisher Scientific) according to the manufacturer's protocol. PCR reaction was performed as follows: 50°C for 2 min; 95°C for 10 min; 95°C for 15 s, 60°C for 1 min, for 40 cycles.

To evaluate the expression of coding genes and precipitated DNA we used the SYBR Green method. RT-qPCR primers (Table S1) were designed by the primer design program Primer3Plus or downloaded from a study by Forouhan et al.[97] First-strand cDNA was synthetized using the High-Capacity cDNA Reverse transcription kit (Thermo Fisher Scientific) following the manufacturer's protocol while precipitated DNA was de-crosslinked (65°C for 1 h), purified using classic phenol-chloroform, followed by ethanol precipitation. RT-qPCR were performed with ABI 7500 Standard RT-qPCR System (Thermo Fisher Scientific). The total reaction volume was 10 μL, including 2 μL 5× Hot FirePol EvaGreen qPCR Mix (Solis BioDyne), 0.6 μL of 10 μM left primer, 0.6 μL of 10 μM right primer, 1 μL template (10 ng/μL), and 4.2 μL of water. Each assay was performed in quadruplicate and using at least three biological replicates. Negative controls without template were added each time. The PCR program started with 2 min at 95°C, followed by 40 cycles of two temperature steps (95°C, 15 s; 60°C, 1 min) and ended with 15 s at 95°C, 1 min at 60°C, 15 s at 95°C and, 15 s at 60°C. The last steps of PCR are performed to acquire the dissociation curve to validate the specificity of the PCR products.

Data analysis was carried on according to ΔΔCt method and statistic was calculated using the t test using unequal variance between samples for miRNA, mRNA, and ChIP RT-qPCR experiments.

DNA extraction for miRNA cloning

To amplify the genomic region encompassing the genes encoding miRNAs, genomic DNA was isolated from the C2C12 cell line. The cells were cultured until they reached 80% of confluence, trypsinized, and centrifuged. Subsequently, the medium was removed, and genomic DNA was extracted using the kit PureLink Genomic DNA Mini Kit (Invitrogen) in accordance with the manufacturer's instructions. Eluted DNA was checked using the NanoDrop One spectrophotometer (Thermo Scientific Scientific) for its quantification and purity (A260/A280 and A260/A230 higher than 1.7).

miRNA cloning

The primers for miRNA cloning were designed to amplify around 500–700 bp region flanking the sequence of the-miRNA. Used primers are described in Figure S7. The PCR reaction was performed as follows: 25 μL of PrimeSTAR Max Premix 2× (Takara Bio), 1 μL of forward primer (10 μM), 1 μL of reverse primer (10 μM), 1 μL DNA (100 ng/μL), 22 μL of Gibco DNase/RNase free water. The thermocycler program used was as follows: activation step (×1) 95°C for 5 min; first PCR cycle (×8) 95°C for 30 s (denaturation), 60°C for 45 s (annealing), 72°C for 90 s; second PCR cycle (×30) 95°C for 30 s (denaturation), 72°C for 70 s (annealing/elongation); final elongation (×1) 72°C for 10 min. Amplicons were verified in an agarose gel of 1.5%. The PCR products were subsequently purified using the NucleoSpin Gel and PCR Clean-up (Macherey-Nagel) and quantified with the NanoDrop One spectrophotometer (Thermo Fisher Scientific) (A260/A280 and A260/A230 higher than 1.7). pCMVmiR-GFP vector (Origene), a specific plasmid for miRNA expression, was linearized with AscI and XhoI restriction enzymes. pCMV-miR-GFP vector (1 μg) was digested in 5 μL of Cutsmart Buffer (New England Biolabs) with 1 μL of AscI (New England Biolabs), and 1 μL of XhoI (New England Biolabs). The reaction was incubated at 37°C for 30 min and the digested vector was run in electrophoresis using low-melting agarose gel to separate vector backbone from excided multi cloning site. The backbone vector was

extracted and purified from the gel with NucleoSpin Gel and PCR Clean-up (Macherey-Nagel) following the manufacturer's protocol. After the purification, the digested product was quantified with the NanoDrop One spectrophotometer (Thermo Fisher Scientific) (A260/A280 and A260/A230 higher than 1.7). To clone prepared amplicons into the purified pCMV-miR-GFP vector, the In-Fusion HD Cloning Kit (Takara Bio) was utilized as follows: 50–100 ng of purified PCR fragment, 100 ng of linearized vector, 2 μL of 5× In-Fusion HD Enzyme premix, H_2O up to 10 μL were mixed and incubated for 15 min at 50°C in a water bath, then placed on ice. Stellar Competent Cells (Takara Bio) were transformed by heat shock following the manufacturer's protocol. After bacteria plating, one colony was expanded to purify the plasmid using GeneJET Plasmid Miniprep Kit (Thermo Fisher Scientific) following the manufacturer's protocol. Plasmids were quantified with the NanoDrop One spectrophotometer (Thermo Fisher Scientific) and sequenced to confirm corrected cloning.

C2C12 cell culture, transfection, and production of stable expressing miRNAs

C2C12 myoblasts were cultured in Dulbecco's modified Eagle's medium with high glucose (Life Technologies) + 10% FBS (Life Technologies) in 10-cm dishes and split every 2 or 3 days before they reached 70% of confluence. C2C12 myoblasts were transfected with 150 nM of mirVana miRNA mimics or scrambled sequence, purchased from Life Technologies. Transfection efficiency of this protocol was estimated on about 60%.[96] Each transfection experiment was independently repeated at least in triplicate.

To evaluate the influence of secreted miRNAs on neurite development, it was necessary to produce cells that overexpress desired miRNA stably. It permits that all cells express the miRNA avoiding the influence of untransfected cells. pCMVmiR-GFP vector (Origene) containing miR-26a, -134a, or -431 gene were used to transfect C2C12 cells. For the stable overexpression of miRNAs, cells were cultured in the proliferative medium without antibiotics 24 h prior to the transfection and 60,000 cells were seeded in 24-well plates (SARSTEDT) in 900 μL DMEM GlutaMAXTM (Thermo Fisher Scientific), 10% FBS (Thermo Fisher Scientific) without antibiotics. The transfection mix (47.5 μL of OptiMEM, 1 μL of 1 μg/μL miRNA plasmid, and 1.5 μL of TransIT-X2 [Mirus]) was added to the cells and the transfection occurred for 24 h. Then, stably transfected cells were selected with 1 mg/mL of the G418/Geneticin antibiotic. After three weeks of selection, antibiotic concentration was reduced to 0.3 mg/mL in order to maintain the selection pressure and reduce cell toxicity for other 2 weeks. After antibiotic selection, G418 was removed and cells were grown in proliferative medium. Cells stable expressing the empty plasmid pCMVmiR was created to be used as a control. miRNA expression on the culture medium of these cells was evaluated using RT-qPCR based on TaqMan probes.

NSC-34 cell transfection

For transfection, NSC34 cells were seeded in triplicate onto collagen I-coated coverslips at a density of 20,000 cells per well in growth medium. After 24 h, the cells were transfected with 1 μg of pCMVmiR-26a-GFP miRNA plasmid using Lipofectamine 3000 reagent (Gibco) according to the manufacturer's instructions. As control, cells were transfected with 1 μg of pCMVmiR-GFP empty vector. Twenty-four hours post-transfection, cell cultures were switched to differentiation medium. Neurite growth was evaluated as previously described.

Validation of miRNA-target interactions

miRNA target predictions are error prone and, therefore, a way to filter them based on the correlation between miRNA and putative target within the cell is needed.[94,98] Since we analyzed secreted miRNAs where targets are not present, we decided to recover miRNA targets using miRTarBase (release 8)[99] and TarBase 8.0[100] databases (Table S2) that contain validated miRNA targets. Since we focused our attention on myoblast differentiation, we considered miRNA target genes associated with striated muscle functions (muscle cell differentiation, muscle tissue development, and muscle cell apoptotic process) according to Biological Process category in the Gene Ontology definitions (Table S3). If databases did not include any information on target-miRNA physical interactions, because interactions were described according to sequencing, microarray, or RT-qPCR experiments, or if interactions were described in a tissue or cells different from skeletal muscle, we performed luciferase assays. In brief, C2C12 cells were transfected with miRNA mimics and 100 pg/mL of pmirGLO Dual-Luciferase miRNA Target Expression Vector (Promega) containing the target sequence or a control sequence (primers for cloning are listed in Table S4). Assays were performed using the Dual-Luciferase Reporter Assay (Promega), measuring firefly and renilla luciferase activities with Turner Designs TD-20/20 Luminometer (DLReady). miRNA transfections were independently replicated at least three times.

Smad4 target identification and chromatin immunoprecipitation PCR

To identify Smad4 targets, we used data presented in a study by Gamart et al.,[101] where a combination of Smad4 ChIP-seq and gene expression analysis after Smad4 depletion in mouse limb buds was used and checked in UCSC Genome Browser the position of Smad4-binding sites in chosen genes. Genes we used to evaluate Smad4 binding in their promoter regions were inhibitors of DNA binding 1 (Id1: Smad4 binding site in the chr2:152576577–152576583), leucine rich repeat containing G protein coupled receptor 5 (Lgr5: Smad4 binding site in the chr10:115431572–115431578), and kinesin family member 7 (Kif7: Smad4 binding site in the chr7:79365377–79365383).

Before the immunoprecipitation cells were cross-linked with PBS 1% formaldehyde for 10 min, they were harvested and lysates were sonicated to an average DNA fragment length of 200–400 bp using the Bioruptor sonicator (Diagenode). The experiment was conducted using 15 μg of chromatin and 5–8 μg of anti-mouse Smad4 (B-8) (Santa Cruz, sc-7966) or anti-mouse IgG isotype control (Cell Signaling Technology, 5415 s). Briefly, chromatin was precleared

by adding 50 μL Protein A/G PLUS-Agarose (Santa Crus, sc-2003) and incubated for 30 min at 4°C. After the solution was centrifugated at full speed for 5 min at 4°C, the supernatant was transferred to a new tube where the primary antibody was added. After an overnight incubation at 4°C, 50 μL of Protein A/G PLUS-Agarose was added and incubated for 2 h at 4°C. Beads were harvested by centrifugation at 12,000 rpm for 20 s. Beads were washed twice with 1 mL of Lysis Buffer High Salt (Santa Cruz; sc-45001) and other two times with Wash Buffer (Santa Cruz; sc-45002). Beads were resuspended in the Elution Buffer (Santa Cruz; sc-45003). DNA samples were purified and subjected to quantitative real-time PCR as previously described. As negative control of precipitation, in addition to the IgG isotype antibody, a real-time PCR against a DNA region without Smad4 binding sites was used (Table S1).

Statistical analysis

Data were analyzed using Origin 2018 (version 9.5) or GraphPad (version 8.0.2) softwares. Statistical analyses were performed as indicated in the figure legends. The significant level was established at $p < 0.05$. Microarray data were analyzed by Kruskal-Wallis test to identify differentially expressed miRNAs setting $p < 0.05$ as cut-off value. All analyses were conducted in double-blind manner.

DATA AVAILABILITY

Transcriptomic data were deposited in the Gene Expression Omnibus database (GSE274702).

ACKNOWLEDGMENTS

We thank the animal care facility of the Polo Vallisneri (University of Padova) for their support in maintenance of mice used in this work and Dr. Michele Gintoli of CNR of Italy, Neuroscience Institute, Padova for helping with Leica Stellaris microscope. C.P. was supported by a fellowship granted from Department of Biomedical Sciences. We thank the University of Padova, The Cariplo Foundation, and the intramural Seed for fundings. This work was supported by grants from the University of Padova (BIRD 202151/20) to A.B. and by grants from The Cariplo Foundation (2016-1006) and the intramural Seed 2019 to S.C. All aspects of mouse maintenance and experiments were carried out in accordance with European and Italian (D.L. 26/2014) laws concerning the care and use of laboratory animals. All experimental procedures and animal care protocols were approved by the Italian Ministry of Health (authorization N. 305/2017-PR for SOD1 mice and N. 248/2024-PR for FUS mice) and by the Ethical Committee for animal care and use of the University of Padova (OPBA). All efforts were made to minimize animal suffering and reduce the number of animals used in the experiments.

AUTHOR CONTRIBUTIONS

Conceptualization, C.P., M.L.M., and S.C.; methodology, C.P., M.L.M., S.C., R.S.B., R.S., S.S., C.M., B.P., L.P., L.C., and V.B.; validation, C.P., A.B., M.L.M., S.C., R.S., and S.S.; formal analysis, C.P., M.L.M., S.C., R.S., A.B., and R.S.B.; resources, A.B. and S.C.; writing – original draft preparation, C.P., M.L.M., and S.C.; writing – review and editing, C.P., M.L.M., R.S., S.C., R.S.B., and A.B.; supervision, C.P., M.L.M., and S.C.; funding acquisition, A.B. and S.C. All authors have read and agreed to the published version of the manuscript.

DECLARATION OF INTERESTS

The authors declare no competing interests.

SUPPLEMENTAL INFORMATION

Supplemental information can be found online at https://doi.org/10.1016/j.omtn.2025.102581.

REFERENCES

1. Longinetti, E., and Fang, F. (2019). Epidemiology of amyotrophic lateral sclerosis: an update of recent literature. Curr. Opin. Neurol. *32*, 771–776. https://doi.org/10.1097/WCO.0000000000000730.

2. Cleveland, D.W., and Rothstein, J.D. (2001). From Charcot to Lou Gehrig: deciphering selective motor neuron death in ALS. Nat. Rev. Neurosci. *2*, 806–819. https://doi.org/10.1038/35097565.

3. Taylor, J.P., Brown, R.H., and Cleveland, D.W. (2016). Decoding ALS: From genes to mechanism. Nature *539*, 197–206. https://doi.org/10.1038/nature20413.

4. Hardiman, O., Al-Chalabi, A., Chio, A., Corr, E.M., Logroscino, G., Robberecht, W., Shaw, P.J., Simmons, Z., and van den Berg, L.H. (2017). Amyotrophic lateral sclerosis. Nat. Rev. Dis. Primers *3*, 17071. https://doi.org/10.1038/nrdp.2017.71.

5. Rosen, D.R., Siddique, T., Patterson, D., Figlewicz, D.A., Sapp, P., Hentati, A., Donaldson, D., Goto, J., O'Regan, J.P., Deng, H.X., et al. (1993). Mutations in Cu/Zn superoxide dismutase gene are associated with familial amyotrophic lateral sclerosis. Nature *362*, 59–62. https://doi.org/10.1038/362059a0.

6. Goutman, S.A., Hardiman, O., Al-Chalabi, A., Chió, A., Savelieff, M.G., Kiernan, M.C., and Feldman, E.L. (2022). Emerging insights into the complex genetics and pathophysiology of amyotrophic lateral sclerosis. Lancet Neurol. *21*, 465–479. https://doi.org/10.1016/S1474-4422(21)00414-2.

7. Mathis, S., Goizet, C., Soulages, A., Vallat, J.-M., and Masson, G.L. (2019). Genetics of amyotrophic lateral sclerosis: A review. J. Neurol. Sci. *399*, 217–226. https://doi.org/10.1016/j.jns.2019.02.030.

8. Gurney, M.E., Pu, H., Chiu, A.Y., Dal Canto, M.C., Polchow, C.Y., Alexander, D.D., Caliendo, J., Hentati, A., Kwon, Y.W., Deng, H.X., et al. (1994). Motor neuron degeneration in mice that express a human Cu,Zn superoxide dismutase mutation. Sci. Technol. Humanit. *264*, 1772–1775. https://doi.org/10.1126/science.8209258.

9. Webster, C.P., Smith, E.F., Shaw, P.J., and De Vos, K.J. (2017). Protein Homeostasis in Amyotrophic Lateral Sclerosis: Therapeutic Opportunities? Front. Mol. Neurosci. *10*, 123. https://doi.org/10.3389/fnmol.2017.00123.

10. Tank, E.M., Figueroa-Romero, C., Hinder, L.M., Bedi, K., Archbold, H.C., Li, X., Weskamp, K., Safren, N., Paez-Colasante, X., Pacut, C., et al. (2018). Abnormal RNA stability in amyotrophic lateral sclerosis. Nat. Commun. *9*, 2845. https://doi.org/10.1038/s41467-018-05049-z.

11. Castellanos-Montiel, M.J., Chaineau, M., and Durcan, T.M. (2020). The Neglected Genes of ALS: Cytoskeletal Dynamics Impact Synaptic Degeneration in ALS. Front. Cell. Neurosci. *14*, 594975. https://doi.org/10.3389/fncel.2020.594975.

12. Peggion, C., Scalcon, V., Massimino, M.L., Nies, K., Lopreiato, R., Rigobello, M.P., and Bertoli, A. (2022). SOD1 in ALS: Taking Stock in Pathogenic Mechanisms and the Role of Glial and Muscle Cells. Antioxidants *11*, 614. https://doi.org/10.3390/antiox11040614.

13. Weishaupt, J.H., Hyman, T., and Dikic, I. (2016). Common Molecular Pathways in Amyotrophic Lateral Sclerosis and Frontotemporal Dementia. Trends Mol. Med. *22*, 769–783. https://doi.org/10.1016/j.molmed.2016.07.005.

14. Ilieva, H., Polymenidou, M., and Cleveland, D.W. (2009). Non–cell autonomous toxicity in neurodegenerative disorders: ALS and beyond. J. Cell Biol. *187*, 761–772. https://doi.org/10.1083/jcb.200908164.

15. Pansarasa, O., Rossi, D., Berardinelli, A., and Cereda, C. (2014). Amyotrophic Lateral Sclerosis and Skeletal Muscle: An Update. Mol. Neurobiol. *49*, 984–990. https://doi.org/10.1007/s12035-013-8578-4.

16. Van Harten, A.C.M., Phatnani, H., and Przedborski, S. (2021). Non-cell-autonomous pathogenic mechanisms in amyotrophic lateral sclerosis. Trends Neurosci. *44*, 658–668. https://doi.org/10.1016/j.tins.2021.04.008.

17. Schweingruber, C., and Hedlund, E. (2022). The Cell Autonomous and Non-Cell Autonomous Aspects of Neuronal Vulnerability and Resilience in Amyotrophic Lateral Sclerosis. Biology (Basel) *11*, 1191. https://doi.org/10.3390/biology11081191.

18. Galbiati, M., Crippa, V., Rusmini, P., Cristofani, R., Cicardi, M.E., Giorgetti, E., Onesto, E., Messi, E., and Poletti, A. (2014). ALS-related misfolded protein management in motor neurons and muscle cells. Neurochem. Int. *79*, 70–78. https://doi.org/10.1016/j.neuint.2014.10.007.

19. Quessada, C., Bouscary, A., René, F., Valle, C., Ferri, A., Ngo, S.T., and Loeffler, J.P. (2021). Skeletal muscle metabolism: Origin or prognostic factor for amyotrophic lateral sclerosis (als) development? Cells *10*, 1449. https://doi.org/10.3390/cells10061449.

20. Moloney, E.B., de Winter, F., and Verhaagen, J. (2014). ALS as a distal axonopathy: molecular mechanisms affecting neuromuscular junction stability in the presymptomatic stages of the disease. Front. Neurosci. *8*, 252. https://doi.org/10.3389/fnins.2014.00252.

21. Bell, L.C., Fuentes, A.E., Healey, D.R., Chao, R., Bakkar, N., Sirianni, R.W., Medina, D.X., Bowser, R.P., Ladha, S.S., Semmineh, N.B., et al. (2022). Longitudinal evaluation of myofiber microstructural changes in a preclinical ALS model using the transverse relaxivity at tracer equilibrium (TRATE): A preliminary study. Magn. Reson. Imaging *85*, 217–221. https://doi.org/10.1016/j.mri.2021.10.036.

22. Manzano, R., Toivonen, J.M., Oliván, S., Calvo, A.C., Moreno-Igoa, M., Muñoz, M. J., Zaragoza, P., García-Redondo, A., and Osta, R. (2011). Altered expression of myogenic regulatory factors in the mouse model of amyotrophic lateral sclerosis. Neurodegener. Dis. *8*, 386–396. https://doi.org/10.1159/000324159.

23. Manzano, R., Toivonen, J.M., Calvo, A.C., Oliván, S., Zaragoza, P., Rodellar, C., Montarras, D., and Osta, R. (2013). Altered *in vitro* proliferation of mouse SOD1-G93A skeletal muscle satellite cells. Neurodegener. Dis. *11*, 153–164. https://doi.org/10.1159/000338061.

24. Pradat, P.-F., Barani, A., Wanschitz, J., Dubourg, O., Lombès, A., Bigot, A., Mouly, V., Bruneteau, G., Salachas, F., Lenglet, T., et al. (2011). Abnormalities of satellite cells function in amyotrophic lateral sclerosis. Amyotroph Lateral Scler. *12*, 264–271. https://doi.org/10.3109/17482968.2011.566618.

25. Scaramozza, A., Marchese, V., Papa, V., Salaroli, R., Sorarù, G., Angelini, C., and Cenacchi, G. (2014). Skeletal muscle satellite cells in amyotrophic lateral sclerosis. Ultrastruct. Pathol. *38*, 295–302. https://doi.org/10.3109/01913123.2014.937842.

26. Doppler, K., Mittelbronn, M., and Bornemann, A. (2008). Myogenesis in human denervated muscle biopsies. Muscle Nerve *37*, 79–83. https://doi.org/10.1002/mus.20902.

27. Verma, S., Khurana, S., Vats, A., Sahu, B., Ganguly, N.K., Chakraborti, P., Gourie-Devi, M., and Taneja, V. (2022). Neuromuscular Junction Dysfunction in Amyotrophic Lateral Sclerosis. Mol. Neurobiol. *59*, 1502–1527. https://doi.org/10.1007/s12035-021-02658-6.

28. Vicente-García, C., Hernández-Camacho, J.D., and Carvajal, J.J. (2022). Regulation of myogenic gene expression. Exp. Cell Res. *419*, 113299. https://doi.org/10.1016/j.yexcr.2022.113299.

29. Horak, M., Novak, J., and Bienertova-Vasku, J. (2016). Muscle-specific microRNAs in skeletal muscle development. Dev. Biol. *410*, 1–13. https://doi.org/10.1016/j.ydbio.2015.12.013.

30. Stella, R., Bonadio, R.S., Cagnin, S., Andreotti, R., Massimino, M.L., Bertoli, A., and Peggion, C. (2023). Secreted Metabolome of ALS-Related hSOD1(G93A) Primary Cultures of Myocytes and Implications for Myogenesis. Cells *12*, 2751. https://doi.org/10.3390/cells12232751.

31. Knight, J.D., and Kothary, R. (2011). The myogenic kinome: protein kinases critical to mammalian skeletal myogenesis. Skelet. Muscle *1*, 29. https://doi.org/10.1186/2044-5040-1-29.

32. de Angelis, L., Zhao, J., Andreucci, J.J., Olson, E.N., Cossu, G., and McDermott, J.C. (2005). Regulation of vertebrate myotome development by the p38 MAP kinase-MEF2 signaling pathway. Dev. Biol. *283*, 171–179. https://doi.org/10.1016/j.ydbio.2005.04.009.

33. Keren, A., Bengal, E., and Frank, D. (2005). p38 MAP kinase regulates the expression of XMyf5 and affects distinct myogenic programs during Xenopus development. Dev. Biol. *288*, 73–86. https://doi.org/10.1016/j.ydbio.2005.09.020.

34. Gardner, S., Anguiano, M., and Rotwein, P. (2012). Defining Akt actions in muscle differentiation. Am. J. Physiol. Cell Physiol. *303*, C1292–C1300. https://doi.org/10.1152/ajpcell.00259.2012.

35. Chen, A.E., Ginty, D.D., and Fan, C.-M. (2005). Protein kinase A signalling via CREB controls myogenesis induced by Wnt proteins. Nature *433*, 317–322. https://doi.org/10.1038/nature03126.

36. Ma, T.C., Barco, A., Ratan, R.R., and Willis, D.E. (2014). cAMP-responsive Element-binding Protein (CREB) and cAMP Co-regulate Activator Protein 1 (AP1)-dependent Regeneration-associated Gene Expression and Neurite Growth. J. Biol. Chem. *289*, 32914–32925. https://doi.org/10.1074/jbc.M114.582460.

37. Simon, C.M., Rauskolb, S., Gunnersen, J.M., Holtmann, B., Drepper, C., Dombert, B., Braga, M., Wiese, S., Jablonka, S., Pühringer, D., et al. (2015). Dysregulated IGFBP5 expression causes axon degeneration and motoneuron loss in diabetic neuropathy. Acta Neuropathol. *130*, 373–387. https://doi.org/10.1007/s00401-015-1446-8.

38. Dey, B.K., Gagan, J., Yan, Z., and Dutta, A. (2012). miR-26a is required for skeletal muscle differentiation and regeneration in mice. Genes Dev. *26*, 2180–2191. https://doi.org/10.1101/gad.198085.112.

39. Fu, X., Wang, H., and Hu, P. (2015). Stem cell activation in skeletal muscle regeneration. Cell. Mol. Life Sci. *72*, 1663–1677. https://doi.org/10.1007/s00018-014-1819-5.

40. Ge, J., Xue, Z., Shu, S., Yu, L., Qin, R., Tao, W., Liu, P., Dong, X., Lan, Z., Bao, X., et al. (2023). MiR-431 attenuates synaptic plasticity and memory deficits in APPswe/PS1dE9 mice. JCI Insight *8*, e166270. https://doi.org/10.1172/jci.insight.166270.

41. Schratt, G.M., Tuebing, F., Nigh, E.A., Kane, C.G., Sabatini, M.E., Kiebler, M., and Greenberg, M.E. (2006). A brain-specific microRNA regulates dendritic spine development. Nature *439*, 283–289. https://doi.org/10.1038/nature04367.

42. Christensen, M., Larsen, L.A., Kauppinen, S., and Schratt, G. (2010). Recombinant adeno-associated virus-mediated microRNA delivery into the postnatal mouse brain reveals a role for miR-134 in dendritogenesis *in vivo*. Front. Neural Circuits *3*, 16. https://doi.org/10.3389/neuro.04.016.2009.

43. Clement, A.M., Nguyen, M.D., Roberts, E.A., Garcia, M.L., Boillée, S., Rule, M., McMahon, A.P., Doucette, W., Siwek, D., Ferrante, R.J., et al. (2003). Wild-type nonneuronal cells extend survival of SOD1 mutant motor neurons in ALS mice. Sci. Technol. Humanit. *302*, 113–117. https://doi.org/10.1126/science.1086071.

44. Dobrowolny, G., Aucello, M., Rizzuto, E., Beccafico, S., Mammucari, C., Boncompagni, S., Belia, S., Wannenes, F., Nicoletti, C., Del Prete, Z., et al. (2008). Skeletal muscle is a primary target of SOD1G93A-mediated toxicity. Cell Metab. *8*, 425–436. https://doi.org/10.1016/j.cmet.2008.09.002.

45. Dobrowolny, G., Giacinti, C., Pelosi, L., Nicoletti, C., Winn, N., Barberi, L., Molinaro, M., Rosenthal, N., and Musarò, A. (2005). Muscle expression of a local Igf-1 isoform protects motor neurons in an ALS mouse model. J. Cell Biol. *168*, 193–199. https://doi.org/10.1083/jcb.200407021.

46. Wong, M., and Martin, L.J. (2010). Skeletal muscle-restricted expression of human SOD1 causes motor neuron degeneration in transgenic mice. Hum. Mol. Genet. *19*, 2284–2302. https://doi.org/10.1093/hmg/ddq106.

47. Fischer, L.R., Culver, D.G., Tennant, P., Davis, A.A., Wang, M., Castellano-Sanchez, A., Khan, J., Polak, M.A., and Glass, J.D. (2004). Amyotrophic lateral sclerosis is a distal axonopathy: evidence in mice and man. Exp. Neurol. *185*, 232–240. https://doi.org/10.1016/j.expneurol.2003.10.004.

48. Cykowski, M.D., Dickson, D.W., Powell, S.Z., Arumanayagam, A.S., Rivera, A.L., and Appel, S.H. (2019). Dipeptide repeat (DPR) pathology in the skeletal muscle of ALS patients with C9ORF72 repeat expansion. Acta Neuropathol. *138*, 667–670. https://doi.org/10.1007/s00401-019-02050-8.

49. Chargé, S.B.P., and Rudnicki, M.A. (2004). Cellular and molecular regulation of muscle regeneration. Physiol. Rev. *84*, 209–238. https://doi.org/10.1152/physrev.00019.2003.

50. Goudenege, S., Pisani, D.F., Wdziekonski, B., Di Santo, J.P., Bagnis, C., Dani, C., and Dechesne, C.A. (2009). Enhancement of Myogenic and Muscle Repair Capacities of Human Adipose–derived Stem Cells With Forced Expression of MyoD. Mol. Ther. *17*, 1064–1072. https://doi.org/10.1038/mt.2009.67.

51. Asfour, H.A., Allouh, M.Z., and Said, R.S. (2018). Myogenic regulatory factors: The orchestrators of myogenesis after 30 years of discovery. Exp. Biol. Med. *243*, 118–128. https://doi.org/10.1177/1535370217749494.

52. Jensen, L., Jørgensen, L.H., Bech, R.D., Frandsen, U., and Schrøder, H.D. (2016). Skeletal Muscle Remodelling as a Function of Disease Progression in Amyotrophic Lateral Sclerosis. BioMed Res. Int. *2016*, 1–12. https://doi.org/10.1155/2016/5930621.

53. Brennan, C.M., Emerson, C.P., Owens, J., and Christoforou, N. (2021). p38 MAPKs — roles in skeletal muscle physiology, disease mechanisms, and as

potential therapeutic targets. JCI Insight *6*, e149915. https://doi.org/10.1172/jci.insight.149915.

54. Berkes, C.A., Bergstrom, D.A., Penn, B.H., Seaver, K.J., Knoepfler, P.S., and Tapscott, S.J. (2004). Pbx marks genes for activation by MyoD indicating a role for a homeodomain protein in establishing myogenic potential. Mol. Cell *14*, 465–477. https://doi.org/10.1016/s1097-2765(04)00260-6.

55. Liu, Q.-C., Zha, X.-H., Faralli, H., Yin, H., Louis-Jeune, C., Perdiguero, E., Pranckeviciene, E., Muñoz-Cànoves, P., Rudnicki, M.A., Brand, M., et al. (2012). Comparative expression profiling identifies differential roles for Myogenin and p38α MAPK signaling in myogenesis. J. Mol. Cell Biol. *4*, 386–397. https://doi.org/10.1093/jmcb/mjs045.

56. Briata, P., Forcales, S.V., Ponassi, M., Corte, G., Chen, C.-Y., Karin, M., Puri, P.L., and Gherzi, R. (2005). p38-Dependent Phosphorylation of the mRNA Decay-Promoting Factor KSRP Controls the Stability of Select Myogenic Transcripts. Mol. Cell *20*, 891–903. https://doi.org/10.1016/j.molcel.2005.10.021.

57. Stewart, R., Flechner, L., Montminy, M., and Berdeaux, R. (2011). CREB Is Activated by Muscle Injury and Promotes Muscle Regeneration. PLoS One *6*, e24714. https://doi.org/10.1371/journal.pone.0024714.

58. Serrano, A.L., Baeza-Raja, B., Perdiguero, E., Jardí, M., and Muñoz-Cánoves, P. (2008). Interleukin-6 is an essential regulator of satellite cell-mediated skeletal muscle hypertrophy. Cell Metab. *7*, 33–44. https://doi.org/10.1016/j.cmet.2007.11.011.

59. Li, L., Chen, Y., Nie, L., Ding, X., Zhang, X., Zhao, W., Xu, X., Kyei, B., Dai, D., Zhan, S., et al. (2019). MyoD-induced circular RNA CDR1as promotes myogenic differentiation of skeletal muscle satellite cells. Biochim. Biophys. Acta. Gene Regul. Mech. *1862*, 807–821. https://doi.org/10.1016/j.bbagrm.2019.07.001.

60. Giudice, J., and Taylor, J.M. (2017). Muscle as a paracrine and endocrine organ. Curr. Opin. Pharmacol. *34*, 49–55. https://doi.org/10.1016/j.coph.2017.05.005.

61. Pedersen, B.K., and Febbraio, M.A. (2012). Muscles, exercise and obesity: skeletal muscle as a secretory organ. Nat. Rev. Endocrinol. *8*, 457–465. https://doi.org/10.1038/nrendo.2012.49.

62. Lindegaard, B., Matthews, V.B., Brandt, C., Hojman, P., Allen, T.L., Estevez, E., Watt, M.J., Bruce, C.R., Mortensen, O.H., Syberg, S., et al. (2013). Interleukin-18 activates skeletal muscle AMPK and reduces weight gain and insulin resistance in mice. Diabetes *62*, 3064–3074. https://doi.org/10.2337/db12-1095.

63. Henningsen, J., Rigbolt, K.T.G., Blagoev, B., Pedersen, B.K., and Kratchmarova, I. (2010). Dynamics of the Skeletal Muscle Secretome during Myoblast Differentiation. Mol. Cell. Proteomics *9*, 2482–2496. https://doi.org/10.1074/mcp.M110.002113.

64. Meroni, M., Crippa, V., Cristofani, R., Rusmini, P., Cicardi, M.E., Messi, E., Piccolella, M., Tedesco, B., Ferrari, V., Sorarù, G., et al. (2019). Transforming growth factor beta 1 signaling is altered in the spinal cord and muscle of amyotrophic lateral sclerosis mice and patients. Neurobiol. Aging *82*, 48–59. https://doi.org/10.1016/j.neurobiolaging.2019.07.001.

65. Dobrowolny, G., Aucello, M., Molinaro, M., and Musarò, A. (2008). Local expression of mIgf-1 modulates ubiquitin, caspase and CDK5 expression in skeletal muscle of an ALS mouse model. Neurol. Res. *30*, 131–136. https://doi.org/10.1179/174313208X281235.

66. Van Dyke, J.M., Smit-Oistad, I.M., Macrander, C., Krakora, D., Meyer, M.G., and Suzuki, M. (2016). Macrophage-mediated inflammation and glial response in the skeletal muscle of a rat model of familial amyotrophic lateral sclerosis (ALS). Exp. Neurol. *277*, 275–282. https://doi.org/10.1016/j.expneurol.2016.01.008.

67. Malacarne, C., Galbiati, M., Giagnorio, E., Cavalcante, P., Salerno, F., Andreetta, F., Cagnoli, C., Taiana, M., Nizzardo, M., Corti, S., et al. (2021). Dysregulation of Muscle-Specific MicroRNAs as Common Pathogenic Feature Associated with Muscle Atrophy in ALS, SMA and SBMA: Evidence from Animal Models and Human Patients. Int. J. Mol. Sci. *22*, 5673. https://doi.org/10.3390/ijms22115673.

68. Lam, N.T., Gartz, M., Thomas, L., Haberman, M., and Strande, J.L. (2020). Influence of microRNAs and exosomes in muscle health and diseases. J. Muscle Res. Cell Motil. *41*, 269–284. https://doi.org/10.1007/s10974-019-09555-5.

69. Anakor, E., Milla, V., Connolly, O., Martinat, C., Pradat, P.F., Dumonceaux, J., Duddy, W., and Duguez, S. (2022). The Neurotoxicity of Vesicles Secreted by ALS Patient Myotubes Is Specific to Exosome-Like and Not Larger Subtypes. Cells *11*, 845. https://doi.org/10.3390/cells11050845.

70. Arroyo, J.D., Chevillet, J.R., Kroh, E.M., Ruf, I.K., Pritchard, C.C., Gibson, D.F., Mitchell, P.S., Bennett, C.F., Pogosova-Agadjanyan, E.L., Stirewalt, D.L., et al. (2011). Argonaute2 complexes carry a population of circulating microRNAs independent of vesicles in human plasma. Proc. Natl. Acad. Sci. USA *108*, 5003–5008. https://doi.org/10.1073/pnas.1019055108.

71. Zhang, A., Wang, H., Wang, B., Yuan, Y., Klein, J.D., and Wang, X.H. (2019). Exogenous miR-26a suppresses muscle wasting and renal fibrosis in obstructive kidney disease. FASEB J. *33*, 13590–13601. https://doi.org/10.1096/fj.201900884R.

72. Lee, K.-P., Shin, Y.J., Panda, A.C., Abdelmohsen, K., Kim, J.Y., Lee, S.-M., Bahn, Y. J., Choi, J.Y., Kwon, E.-S., Baek, S.-J., et al. (2015). miR-431 promotes differentiation and regeneration of old skeletal muscle by targeting Smad4. Genes Dev. *29*, 1605–1617. https://doi.org/10.1101/gad.263574.115.

73. Wu, R., Li, H., Zhai, L., Zou, X., Meng, J., Zhong, R., Li, C., Wang, H., Zhang, Y., and Zhu, D. (2015). MicroRNA-431 accelerates muscle regeneration and ameliorates muscular dystrophy by targeting Pax7 in mice. Nat. Commun. *6*, 7713. https://doi.org/10.1038/ncomms8713.

74. Su, Y., Deng, M.-F., Xiong, W., Xie, A.-J., Guo, J., Liang, Z.-H., Hu, B., Chen, J.-G., Zhu, X., Man, H.-Y., et al. (2019). MicroRNA-26a/Death-Associated Protein Kinase 1 Signaling Induces Synucleinopathy and Dopaminergic Neuron Degeneration in Parkinson's Disease. Biol. Psychiatry *85*, 769–781. https://doi.org/10.1016/j.biopsych.2018.12.008.

75. Zhang, H., Lu, X., Hao, Y., Tang, L., and He, Z. (2020). MicroRNA-26a-5p alleviates neuronal apoptosis and brain injury in intracerebral hemorrhage by targeting RAN binding protein 9. Acta Histochem. *122*, 151571. https://doi.org/10.1016/j.acthis.2020.151571.

76. Zhang, Y., Su, Z., Liu, H.-L., Li, L., Wei, M., Ge, D.-J., and Zhang, Z.-J. (2018). Effects of miR-26a-5p on neuropathic pain development by targeting MAPK6 in in CCI rat models. Biomed. Pharmacother. *107*, 644–649. https://doi.org/10.1016/j.biopha.2018.08.005.

77. Allander, S.V., Coleman, M., Luthman, H., and Powell, D.R. (1997). Chicken Insulin-like Growth Factor Binding Protein (IGFBP)-5: Conservation of IGFBP-5 Structure and Expression During Evolution. Comp. Biochem. Physiol. B Biochem. Mol. Biol. *116*, 477–483. https://doi.org/10.1016/S0305-0491(96)00289-1.

78. James, P.L., Jones, S.B., Busby, W.H., Clemmons, D.R., and Rotwein, P. (1993). A highly conserved insulin-like growth factor-binding protein (IGFBP-5) is expressed during myoblast differentiation. J. Biol. Chem. *268*, 22305–22312. https://doi.org/10.1016/S0021-9258(18)41529-3.

79. Salih, D.A.M., Tripathi, G., Holding, C., Szestak, T.A.M., Gonzalez, M.I., Carter, E. J., Cobb, L.J., Eisemann, J.E., and Pell, J.M. (2004). Insulin-like growth factor-binding protein 5 (Igfbp5) compromises survival, growth, muscle development, and fertility in mice. Proc. Natl. Acad. Sci. USA *101*, 4314–4319. https://doi.org/10.1073/pnas.0400230101.

80. Wu, D., and Murashov, A.K. (2013). MicroRNA-431 regulates axon regeneration in mature sensory neurons by targeting the Wnt antagonist Kremen1. Front. Mol. Neurosci. *6*, 35. https://doi.org/10.3389/fnmol.2013.00035.

81. Liu, Y., Wang, J., Zhou, X., Cao, H., Zhang, X., Huang, K., Li, X., Yang, G., and Shi, X. (2020). miR-324-5p Inhibits C2C12 cell Differentiation and Promotes Intramuscular Lipid Deposition through lncDUM and PM20D1. Mol. Ther. Nucleic Acids *22*, 722–732. https://doi.org/10.1016/j.omtn.2020.09.037.

82. Dmitriev, P., Barat, A., Polesskaya, A., O'Connell, M.J., Robert, T., Dessen, P., Walsh, T.A., Lazar, V., Turki, A., Carnac, G., et al. (2013). Simultaneous miRNA and mRNA transcriptome profiling of human myoblasts reveals a novel set of myogenic differentiation-associated miRNAs and their target genes. BMC Genom. *14*, 265. https://doi.org/10.1186/1471-2164-14-265.

83. Silva, G.J.J., Bye, A., el Azzouzi, H., and Wisløff, U. (2017). MicroRNAs as Important Regulators of Exercise Adaptation. Prog. Cardiovasc. Dis. *60*, 130–151. https://doi.org/10.1016/j.pcad.2017.06.003.

84. Zhu, R.-Y., Zhang, D., Zou, H.-D., Zuo, X.-S., Zhou, Q.-S., and Huang, H. (2016). MiR-28 inhibits cardiomyocyte survival through suppressing PDK1/Akt/mTOR signaling. In Vitro Cell. Dev. Biol. Anim. *52*, 1020–1025. https://doi.org/10.1007/s11626-016-0065-6.

85. Lamon, S., Zacharewicz, E., Butchart, L.C., Orellana, L., Mikovic, J., Grounds, M.D., and Russell, A.P. (2017). MicroRNA expression patterns in post-natal mouse skeletal muscle development. BMC Genom. *18*, 52. https://doi.org/10.1186/s12864-016-3399-2.

86. Tay, Y.M.-S., Tam, W.-L., Ang, Y.-S., Gaughwin, P.M., Yang, H., Wang, W., Liu, R., George, J., Ng, H.-H., Perera, R.J., et al. (2008). MicroRNA-134 modulates the differentiation of mouse embryonic stem cells, where it causes post-transcriptional attenuation of Nanog and LRH1. Stem Cell. *26*, 17–29. https://doi.org/10.1634/stemcells.2007-0295.

87. Gaughwin, P., Ciesla, M., Yang, H., Lim, B., and Brundin, P. (2011). Stage-specific modulation of cortical neuronal development by Mmu-miR-134. Cereb. Cortex *21*, 1857–1869. https://doi.org/10.1093/cercor/bhq262.

88. Bicker, S., Lackinger, M., Weiß, K., and Schratt, G. (2014). MicroRNA-132, -134, and -138: a microRNA troika rules in neuronal dendrites. Cell. Mol. Life Sci. *71*, 3987–4005. https://doi.org/10.1007/s00018-014-1671-7.

89. Norante, R.P., Massimino, M.L., Lorenzon, P., De Mario, A., Peggion, C., Vicario, M., Albiero, M., Sorgato, M.C., Lopreiato, R., and Bertoli, A. (2017). Generation and validation of novel adeno-associated viral vectors for the analysis of Ca2+ homeostasis in motor neurons. Sci. Rep. *7*, 6521. https://doi.org/10.1038/s41598-017-06919-0.

90. Massimino, M.L., Ferrari, J., Sorgato, M.C., and Bertoli, A. (2006). Heterogeneous PrP C metabolism in skeletal muscle cells. FEBS Lett. *580*, 878–884. https://doi.org/10.1016/j.febslet.2006.01.008.

91. Madison, R.D., McGee, C., Rawson, R., and Robinson, G.A. (2014). Extracellular vesicles from a muscle cell line (C2C12) enhance cell survival and neurite outgrowth of a motor neuron cell line (NSC-34). J. Extracell. Vesicles *3*. https://doi.org/10.3402/jev.v3.22865.

92. Colella, A.D., Chegenii, N., Tea, M.N., Gibbins, I.L., Williams, K.A., and Chataway, T.K. (2012). Comparison of Stain-Free gels with traditional immunoblot loading control methodology. Anal. Biochem. *430*, 108–110. https://doi.org/10.1016/j.ab.2012.08.015.

93. Codolo, G., Toffoletto, M., Chemello, F., Coletta, S., Soler Teixidor, G., Battaggia, G., Munari, G., Fassan, M., Cagnin, S., and de Bernard, M. (2019). Helicobacter pylori Dampens HLA-II Expression on Macrophages via the Up-Regulation of miRNAs Targeting CIITA. Front. Immunol. *10*, 2923. https://doi.org/10.3389/fimmu.2019.02923.

94. Cagnin, S., Brugnaro, M., Millino, C., Pacchioni, B., Troiano, C., Di Sante, M., and Kaludercic, N. (2022). Monoamine Oxidase-Dependent Pro-Survival Signaling in Diabetic Hearts Is Mediated by miRNAs. Cells *11*, 2697. https://doi.org/10.3390/cells11172697.

95. Huang, H.-Y., Lin, Y.-C.-D., Cui, S., Huang, Y., Tang, Y., Xu, J., Bao, J., Li, Y., Wen, J., Zuo, H., et al. (2022). miRTarBase update 2022: an informative resource for experimentally validated miRNA–target interactions. Nucleic Acids Res. *50*, D222–D230. https://doi.org/10.1093/nar/gkab1079.

96. Chemello, F., Grespi, F., Zulian, A., Cancellara, P., Hebert-Chatelain, E., Martini, P., Bean, C., Alessio, E., Buson, L., Bazzega, M., et al. (2019). Transcriptomic Analysis of Single Isolated Myofibers Identifies miR-27a-3p and miR-142-3p as Regulators of Metabolism in Skeletal Muscle. Cell Rep. *26*, 3784–3797.e8. https://doi.org/10.1016/j.celrep.2019.02.105.

97. Forouhan, M., Lim, W.F., Zanetti-Domingues, L.C., Tynan, C.J., Roberts, T.C., Malik, B., Manzano, R., Speciale, A.A., Ellerington, R., Garcia-Guerra, A., et al. (2022). AR cooperates with SMAD4 to maintain skeletal muscle homeostasis. Acta Neuropathol. *143*, 713–731. https://doi.org/10.1007/s00401-022-02428-1.

98. Corso, D., Chemello, F., Alessio, E., Urso, I., Ferrarese, G., Bazzega, M., Romualdi, C., Lanfranchi, G., Sales, G., and Cagnin, S. (2021). MyoData: An expression knowledgebase at single cell/nucleus level for the discovery of coding-noncoding RNA functional interactions in skeletal muscle. Comput. Struct. Biotechnol. J. *19*, 4142–4155. https://doi.org/10.1016/j.csbj.2021.07.020.

99. Huang, H.-Y., Lin, Y.-C.-D., Cui, S., Huang, Y., Tang, Y., Xu, J., Bao, J., Li, Y., Wen, J., Zuo, H., et al. (2022). miRTarBase update 2022: an informative resource for experimentally validated miRNA-target interactions. Nucleic Acids Res. *50*, D222–D230. https://doi.org/10.1093/nar/gkab1079.

100. Karagkouni, D., Paraskevopoulou, M.D., Chatzopoulos, S., Vlachos, I.S., Tastsoglou, S., Kanellos, I., Papadimitriou, D., Kavakiotis, I., Maniou, S., Skoufos, G., et al. (2018). DIANA-TarBase v8: a decade-long collection of experimentally supported miRNA–gene interactions. Nucleic Acids Res. *46*, D239–D245. https://doi.org/10.1093/nar/gkx1141.

101. Gamart, J., Barozzi, I., Laurent, F., Reinhardt, R., Martins, L.R., Oberholzer, T., Visel, A., Zeller, R., and Zuniga, A. (2021). SMAD4 target genes are part of a transcriptional network that integrates the response to BMP and SHH signaling during early limb bud patterning. Development *148*, dev200182. https://doi.org/10.1242/dev.200182.